

Exploring *Citrus sinensis* Phytochemicals as Potential Inhibitors for Breast Cancer Genes BRCA1 and BRCA2 Using Pharmacophore Modeling, Molecular Docking, MD Simulations, and DFT Analysis

Mehreen Zia, Shagufta Parveen, Nusrat Shafiq,* Maryam Rashid, Ariba Farooq, Musaab Dauelbait,* Muhammad Shahab, Ahmad Mohammad Salamatullah, Simone Brogi, and Mohammed Bourhia



Cite This: *ACS Omega* 2024, 9, 2161–2182



Read Online

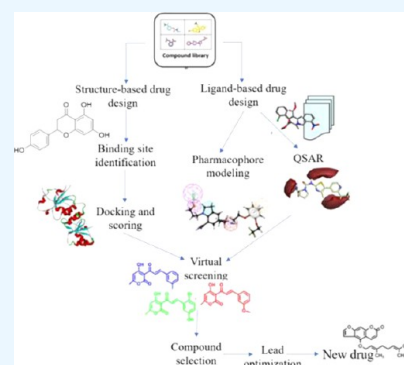
ACCESS |

Metrics & More

Article Recommendations

Supporting Information

ABSTRACT: Background: Structure–activity relationship (SAR) is considered to be an effective *in silico* approach when discovering potential antagonists for breast cancer due to gene mutation. Major challenges are faced by conventional SAR in predicting novel antagonists due to the discovery of diverse antagonistic compounds. Methodology and Results: In predicting breast cancer antagonists, a multistep screening of phytochemicals isolated from the seeds of the *Citrus sinensis* plant was applied using feasible complementary methodologies. A three-dimensional quantitative structure–activity relationship (3D-QSAR) model was developed through the Flare project, in which conformational analysis, pharmacophore generation, and compound alignment were done. Ten hit compounds were obtained through the development of the 3D-QSAR model. For exploring the mechanism of action of active compounds against cocystal inhibitors, molecular docking analysis was done through Molegro software (MVD) to identify lead compounds. Three new proteins, namely, 1T15, 3EU7, and 1T29, displayed the best Moldock scores. The quality of the docking study was assessed by a molecular dynamics simulation. Based on binding affinities to the receptor in the docking studies, three lead compounds (stigmasterol **P8**, epoxybergamottin **P28**, and nobiletin **P29**) were obtained, and they passed through absorption, distribution, metabolism, and excretion (ADME) studies via the SwissADME online service, which proved that **P28** and **P29** were the most active allosteric inhibitors with the lowest toxicity level against breast cancer. Then, density functional theory (DFT) studies were performed to measure the active compound's reactivity, hardness, and softness with the help of Gaussian 09 software. Conclusions: This multistep screening of phytochemicals revealed high-reliability antagonists of breast cancer by 3D-QSAR using flare, docking analysis, and DFT studies. The present study helps in providing a proper guideline for the development of novel inhibitors of BRCA1 and BRCA2.



1. INTRODUCTION

Phytochemicals make up a diverse group of bioactive compounds derived from plants. These compounds possess the potential to combat various health-related diseases. The seeds of the *Citrus sinensis* plant contain phytochemicals that have demonstrated activity against breast cancer and have been analyzed through both *in vivo* and *in vitro* studies.¹ Several phytochemicals in *C. sinensis* are responsible for its biological actions. For instance, epoxybergamottin (Figure 1), isolated

from *C. sinensis* as a natural furanocoumarin, has been shown to be an effective anticancer, antioxidant, and anti-inflammatory compound for more than a decade. Strong evidence from toxicology data supports its role in inhibiting various types of cancer, including leukemia, skin, breast, and lung cancer.²

Nobiletin (Figure 1) belongs to the class of flavonoids, is also considered a plant metabolite, and has been used as an antineoplastic agent for many years. It is moderately soluble in water, while in organic solvents, it is extremely soluble. Attempts to discover antagonists' nobiletin are known as a promising candidate in treating cancer, as it possesses multiple targeting capabilities. It can resist the proliferation and invasion

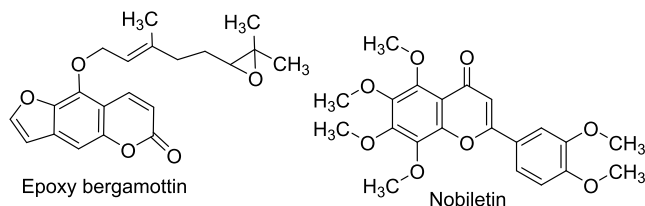
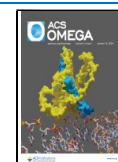


Figure 1. Compounds previously reported from *Citrus sinensis*.

Received: July 15, 2023
Revised: December 12, 2023
Accepted: December 19, 2023
Published: January 3, 2024



of cancer cells.³ Breast cancer is a serious concern and should be detected as soon as possible because earlier diagnosis would lead to fewer problems, and early treatment could also lower the death rate. Isolated phytochemicals from *C. sinensis* seeds have various biological activities, especially beneficial for protecting against cell damage, which can cause cancer.⁴ The abnormal growth of cells within the lining of lobules and ducts leads to breast cancer and should be diagnosed at the initial stage otherwise, it could be fatal.⁵ In the 19th century, scientists identified the gene whose mutation led to breast cancer. Two genes, i.e., breast cancer gene 1 (BRCA1) and breast cancer gene 2 (BRCA2), are known as suppressor genes because they produce proteins that repair the damaged DNA, but when these genes are mutated, they become harmful variants and cause breast cancer.⁶ An individual has two BRCA1 genes located on each chromosome 17, while two BRCA2 genes are located on chromosome 13, responsible for protecting from tumors and cancers until somatic alteration occurs and causes cancer. The process of mutation or alteration could be inherited from the mother or father, and it is important to note that the location of these genes is not present on the sex chromosome. This mutation is a germline mutation, that will occur in all cells of the body of a person.^{7,8} Recent studies have reported that the body mass index (BMI) could be the risk factor for breast cancer in women, especially after menopause. Estrogen biosynthesis is blocked in women carrying BRCA mutation, genomic integrity is decreased in BRCA mutations, while DNA damage is increased and causes tumorigenesis. These BRCA genes are responsible for repairing pathways such as homologous recombination.^{8,9} Scientists revealed that both genes are functionally recessive, so both copies of genes should be mutated for cancer progression. The person having an altered or mutated gene possesses a 50% chance of transferring this gene to the next offspring. Multiple mutations would lead to tumor progression, and inheritance of BRCA1 and BRCA2 mutations causes cancer only when they get a second mutation to trigger the tumor formation.¹⁰ Both BRCA1 and BRCA2 genes also interact with different proteins located in different pathways for recombination and repairing of DNA strands. In the case of mutation, both genes become disturbed, leading to other DNA mutations by repairing DNA in a nonconservative form. Deletions would occur, and the formation of tumorigenesis would take place.¹¹ BRCA1 and BRCA2 have almost similar encoded proteins; therefore, they experience similar functionalities, and due to mutations, interruption of protein translation would occur.¹² Hormonal and particular regional therapies are the most common treatments considered against gene mutation in breast cancer. CDK4/6 inhibitors are also used for blocking cancerous cells in breast cancer. Besides, if anti-HER₂ and endocrine treatment fail, then surgeons move toward immunotherapies.¹³

C. sinensis belongs to the Rutaceae family, which is diverse and comprises 140 genera, including around 1300 citrus species worldwide. *C. sinensis* is considered the most popular and widely cultivated fruit globally, accounting for approximately 70% of all citrus species. While it is native to Asia, recent studies suggest that it is now being produced on a large scale in various countries with Pacific and warm climates. The tree reaches a height of approximately 9–10 m, including branches adorned with large spines. Its leaves are 3–5 mm wide and 6.5–15 cm long.^{14,15} The trees and shrubs of the *C. sinensis* plant are found to be large and evergreen, about 30 in. in height, with dark green elegant leaves. There are 6 whorls

and 5 petals in the flower growing from the axil of the *C. sinensis* plant, including about 25 yellow stamens.¹⁵ The fruit grown is mostly oval in shape (6.5–9.5 cm wide). The fruit comprises different parts such as pericarp (peel), skin, and endocarp (pulp).¹⁶ The ripened fruit of the respective plant produces a sweet pulp and several seeds. *Citrus limon*, *Citrus medica*, *Citrus reticulata*, *Citrus paradisi*, *C. sinensis*, *Citrus grandis*, and *Citrus aurantifolia* are the major *Citrus* species cultivated in subtropical Asia in large production.^{17,18} Various isolated compounds from seeds of *C. sinensis* also possess therapeutic properties in treating breast cancer such as flavonoids, sterols, fatty acids, terpinenes, and carotenoids. Valencia, Hamlin, Perario, and Natal are different varieties of *C. sinensis* plants, commonly used for cough, menstrual disorders, diarrhea, and many other ailments.¹⁹ Research conducted through both in vitro and in vivo studies on BRCA1 and BRCA2 genes has reported that mutations in these genes can lead to the development of breast cancer in mice as well as in humans. In contrast to other species within the *Citrus* family, there has been relatively limited research on *C. sinensis* in recent decades. Previous studies have provided insights into various in vitro and in vivo studies.^{20–25}

Recent research studies revealed new and advanced techniques in finding out therapies and treatments against many diseases such as computer-aided drug designs, which are becoming an effective strategy in this regard.²⁶ CADD when combined with wet laboratories can interpret the process of drug resistance and therapies as well at low cost and reasonable time. Computer-aided drug design has become the latest process in drug development against multiple diseases and has become popular in the pharmaceutical industry in no time. Due to the presence of modern computational tools, the technique helps in the analysis, management as well as modeling of compounds or ligands while traditional methods are risky, expensive, laborious, and time-consuming.^{27,28} Different stages of CADD (Figure 2) include the identification

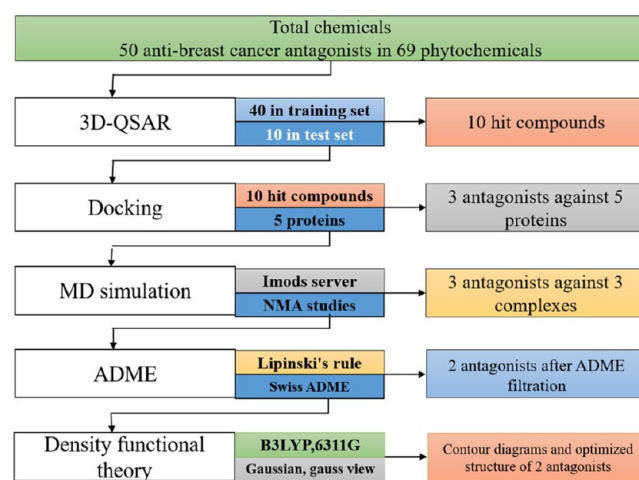


Figure 2. Schematic diagram of the chemical classification process in multistep screening methodology.

of targeted protein, lead discovery, protein validation, and lead optimization.²⁹ This technique explains the binding affinities and the interaction of the protein and ligand. Ligand-based and structure-based drug designs are the types of the latest CADD techniques. In ligand-based drug design, the structure is analyzed and the binding affinity of the compound with the

specific target is predicted with the help of a reference compound.^{30,31} Databases of different known compounds are screened, and in this way, the latest chemical entities are identified by the collection of molecules along with their respective structures. In structure-based design, targets such as enzymes or receptors in the form of 3D structures are used for the optimization process as well as screening of different ligands.^{32,33}

These studies^{18,34,35} showed experimental analysis, while our research was performed again for further clinical trial purposes. The CADD technique was applied to screened compounds taken from the library of 2000 compounds of the seeds of *C. sinensis* (Figure 2), in which different groups of screened compounds such as sterols, carotenoids, terpenoids, flavonoids, fatty acids, and polyphenols were considered. In this study, the role of screened compounds against breast cancer has been discussed with the help of ligand-based and structure-based drug designs. Proteins are involved in the inhibition of different pathways that cause various diseases. So, docking studies have been performed for the interaction of ligands with respective proteins for evaluation of breast cancer. Furthermore, for the prediction of antagonists, different *in silico* methodologies, i.e., density functional theory (DFT) and absorption, distribution, metabolism, and excretion (ADME), have been performed in a stepwise manner.

2. MATERIALS AND METHODS

2.1. Selection of the Data Along with Its Preparation.

A library comprising 2000 compounds (Table S1 in the Supporting Information) from *C. sinensis* species including FDA-proved drugs was selected from the literature as well as from different sites such as PubChem, PubMed, COCONUT, and ZINC databases. About 69 phytochemicals were selected along with their IC_{50} from which 50 phytochemicals as antagonists possess good anti-breast cancer potential from the literature. The chemical structures of phytochemicals were initially in two-dimensional (2D) format and were converted into 3D structures using PerkinElmer software. The CSV file was generated through Microsoft Excel of all of the screened compounds that were exported from the library. The experimental activity of the screened compounds that were divided for the training set as well as for the test set was expressed in IC_{50} , and the $pIC_{50} = -\log(IC_{50})$ formula was used for converting the IC_{50} value into a positive logarithmic scale.

2.2. 3D-QSAR Approach. A series of anticancer compounds with their optimized structures were arranged and exported into a flare tool, i.e., the Field Template module of Forge V6.0 tool, for the establishment of a three-dimensional quantitative structure–activity relationship (3D-QSAR) model. The method of molecular field-based similarity was employed for the purpose of conformational search that designed the pharmacophore template of the ligands. The 3D-QSAR model was generated, which helped in modulating the bioactivity of the molecules.³⁶ The protein selected was 3EQM taken from the Protein Data Bank. The protein selected has a resolution of about 2.90 Å and *Homo sapiens* organism. During visualization, only chain A was considered, while water molecules were deleted. Then, anticancer compounds were randomly divided into training sets along with the test set.

2.3. Parameters for QSAR Development. **2.3.1. Conformation Hunt and Generation of the Pharmacophore Template.** The arrangement of screened phytochemicals

isolated from the *C. sinensis* plant was exported to Flare's worksheet. The training set, as well as the test set, was arranged through the Sphere Exclusion Algorithm. Additionally, the ratio of phytochemicals for anti-breast cancer compounds was taken as 11:40 when phytochemicals were divided into training and test sets. Forge V6.0 software for the Field Template module was applied for visualization of generated fields.³⁷ The conformation hunt was selected as accurate but slow, and from the library of 69 compounds, the information about shape and field was analyzed. The interpretation of the hypothesis was done along with the development of field points as well as a 3D field point pattern. Furthermore, the template represents the bioactive conformation of phytochemicals as well. For the generation of field QSAR, the regression coefficient (r^2), as well as the cross-regression coefficient (q^2), was calculated for each ligand.³⁷

2.3.2. Alignment of Phytochemicals and Development of the 3D-QSAR Model. For defining the descriptors, different molecular properties can be determined with the help of the 3D-QSAR model. This technique covers the maximum number of compounds present in the training set. The pharmacophore template was then imported into the software of Forge v10 for the alignment of compounds. Alignment was done normally for all of the compounds present in training sets. With the help of the generation of the field point-based descriptors, the 3D-QSAR model was developed, and this development was done after the alignment of 50 compounds along with their IC_{50} . During this model, various parameters were taken into consideration, such as 1.0 Å was selected as the distance between different sample points, while the adjustment for Y scrambles was set to 50. Using the forging tool, we achieved a 50% similarity in both the field and volume. The training and test sets are the two integral sets in this model in which our screened compounds were divided. The ratios were taken as 80% and 20%, respectively. IC_{50} of all 50 compounds was converted into pIC_{50} with the formula $pIC_{50} = -\log(IC_{50})$. Alpelisib is the FDA-approved reference drug selected from the literature in comparison to breast cancer compounds.³⁸

2.3.3. Validation of 3D-QSAR Model Development. This model also determines a linear regression model for the active compounds. The regression coefficient (r^2) and cross-validation (q^2) are also determined by this model. For validation of regression, the LOO technique is considered and is also used for optimization of the predicted activity. In this LOOCV technique, each data tended to pass the specific testing process because the repetition of testing as well as training was done for the N number of times; in this way, the test data that were out of the training set were then used for the 3D-QSAR model.³⁹

2.3.4. SAR Activity Atlas Model of Screened Phytochemicals. To get better results and required information about the structure–activity relationship (SAR) of phytochemicals, the model, i.e., activity atlas, was built. The calculation of various molecular fields such as shape, hydrophobicity, and positive and negative electrostatics was done through this influential model, while the condensed representation of selected compounds was done by field points. After the graphical representation of the selected compounds in 3D form is obtained, qualitative information is achieved. Parameters such as activity cliff summary, region explored, and average of actives were obtained through the activity atlas. Favorable shapes of positive and negative electrostatics, active com-

pounds, and hydrophobicity were represented with the help of a cliff summary.^{38,39}

2.4. Exploration of the Action Mechanism of Phytochemicals against Gene Mutation in Breast Cancer by Using an In Silico Approach.

2.4.1. Protein Preparation against Breast Cancer in the Case of Gene Mutation. 3D structures of breast cancer inhibitor proteins for the BRCA1 gene (PDB ID: IT15, 3PXD, 4OFB, 7JZV, 1T29) and the BRCA2 gene (PDB ID: 3EU7, 7LDG, 1IJY) were selected from RCSB, i.e., Protein Data Bank (<http://www.pdb.org>), for docking purpose with active compounds that have been screened from the *C. sinensis* plant. Table 1 shows the

Table 1. PDB IDs for Selected Proteins in the Docking Study against Breast Cancer

PDB ID	ligands	molecule	resolution (Å)	organism
IT15	no bound ligands	breast cancer type 1 susceptibility protein	1.85	<i>Homo sapiens</i>
3PXD	sulfate ion nickel(II) ion	breast cancer type 1 susceptibility protein	2.80	<i>Homo sapiens</i>
4OFB	no bound ligands	breast cancer type 1 susceptibility protein	3.05	<i>Homo sapiens</i>
1T29	no bound ligands	breast cancer type 1 susceptibility protein	2.30	<i>Homo sapiens</i>
3EU7	glycerol	partner and localizer of BRCA2	2.20	<i>Homo sapiens</i>
7JZV	zinc ion	BRCA1, ubiquitin-conjugating enzyme E2 D3	3.90	<i>Homo sapiens</i> synthetic contact
1IJY	no bound ligands	frizzled homologue 8	1.35	<i>Salmonella enterica</i>

proteins selected for this study.⁴⁰ All of the required structures of proteins in PDB were then opened into Discovery Studio software. All of the water molecules along with heteroatoms were removed. Then, ligand binding sites were observed, and then the binding site sphere was also generated. Selected ligands were deleted for docking studies, and the file was saved in SDF format. Molegro software was used for docking studies.⁴¹ The results were obtained in the form of a MolDock score for binding affinities.⁴²

2.4.3. Method of Ligand Preparation. After the screening of ligands from 3D-QSAR, structures of active compounds were drawn by ChemDraw MM2, and MMF9 force fields were applied for the optimization process, and a Mol2 file was generated and then imported to MVD's workspace in Molegro for docking purposes.⁴²

2.4.4. Docking Studies through Molegro Software. In this research, docking was done for the screened phytochemicals through Molegro (MVD) software. The reference drug Alpelisib was selected as a standard drug from PubChem for anti-breast cancer activity for docking with the selected ligands. Before importing the ligand, proteins related to BRCA1 and BRCA2 mutations were taken and imported from the PDB database to MVD's workspace. Most probably, the protein of a single chain and above 1.5 Å is considered the best protein for docking. After importing the SDF file of the protein, Ligands from L1 to L10 were also imported one by one into a workspace for protein–ligand interaction. Before starting the process of docking, all of the cofactors as well as water molecules of the protein were removed from the workspace.

Inhibition poses were also obtained. The highest MolDock rerank score suggests the best poses in the docking process. Through hydrogen bond interaction, the top-rank pose of the compound was obtained along with the best binding affinities in the MolDock score and bond length. It is suggested that parameters such as atom connectivity and bond order along with partial atomic charges should be arranged properly to get valuable results.⁴³

2.5. NMA-Based Simulation. This is also known as validation of docking or assessment of docking quality, which is beneficial in providing evidence for drug repositioning along with drug rescue. This includes docking analysis of drugs or the small-molecule binding process of the particular setting for the available targets. The time duration for the MD simulation on iMODS is almost 5 to 6 min for generation of files, and then it takes 3 to 4 h for the analysis of output files. Basically, the system is an online server in which html file key is used as a processing key with 20 modes while having no clusters and no deformation. We can change the html file with Java or WebGL according to the requirements. From iMODS, we can analyze the normal mode analysis of proteins, visualizing modes, root-mean-square fluctuations, visualization modes, and morphing protein.⁴⁴

In this study, the protein–ligand output file was subjected to MD simulations through iMODS (online server).⁴⁵ The output file of the best protein–ligand interaction was submitted to the server for evaluation of the stability of the complex. Obtained results were presented in appropriate form by using Minitab <https://www.minitab.com/en-us/products/minitab/free-trial/>.

2.6. Molecular Dynamics Simulation (MDS). A molecular dynamics (MD) simulation was performed to investigate the dynamic behavior of proteins upon inhibitor binding at the atomic level. Using the ff19SB force field and the AMBER22 package, a thorough MDS analysis was performed.³⁶ The complexes were constructed and solved using the preparation program Tleap. In this experiment, a solvated octahedral box was utilized. Upon solvating each system using the TIP3P water model with 12 in an octahedral box, the complexes were neutralized by introducing counterions (Na⁺ or Cl⁻). In order to accomplish the aim of relaxing all systems, the energy of each neutralized system was minimized as much as feasible in two steps. These methods included conjugate gradient minimization and steepest descent minimization. The complexes after minimization were heated to 300 K at 50 ps. Then, using a two-step process at constant 1 atm and 300 K, each system was brought to equilibrium. First, a weak constraint was utilized to equilibrate the density at 20 ps. Next, we equilibrated the system for 1 ns without any restrictions. The production phase was then run for 100 ns. The system pressure was monitored using the Berendsen barostat, and the temperature was kept stable using the Langevin thermostat.³⁷ We applied the AMBER22 Particle Mesh Ewald (PME) algorithm to calculate long-range electrostatic interaction. The AMBER22 SHAKE algorithm was used to refine the covalent bonds.³⁸ The MD trajectories were examined by using the AMBER22 CPPRTAJ module. Using PyMol v1.7 and Origin Pro Lab v2020, the interface analysis and graphical representation were completed.

2.5.1. Prime MM-GBSA. The binding energy of the protein that was obtained from the MD simulation has been analyzed through MM-GBSA. MM-GBSA is basically called the molecular mechanics generalized Born model and solvent

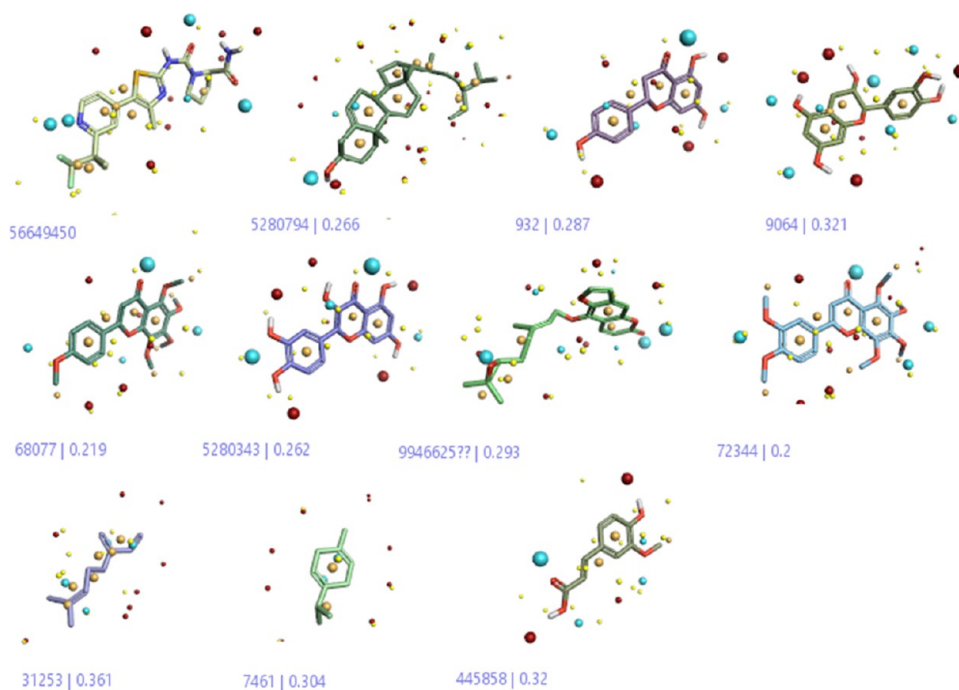


Figure 3. Pharmacophore generation of phytochemicals screened as actives.

accessibility. The basic module of this process used was Schrodinger € for the analysis of the 1T29 complex. The VSGB model was utilized including the OPLS-4 force field and implicit solvent model.⁴⁶

2.7. ADME Study and Toxicity Determination of Selected Compounds. In the computational study, ADME is the drug metabolism process, and its study has gained much attention in carrying out useful calculations. The ADME study was done to identify the ADME problems that occur in predicting the hit compounds and also to resolve failures that appear during clinical analysis. For the determination of the drug ability of the molecule, a significant rule, i.e., Lipinski's rule of five, is being considered. For this study, a valuable tool, i.e., SwissADME <http://www.swissadme.ch/> was used to find out the quantitative information for the disposition of a drug.³⁸ To determine the safety of the selected compounds, the library was checked for toxicity also. Drug development with poor pharmacokinetic and safety measures could be a significant hurdle for the researchers. So, for minimization of these risks, ADME analysis was applied.⁴⁷

2.7.1. Toxicity Prediction. For toxicity prediction, ProTox-II, a web server, gives valuable information about the toxicological profile of isolated compounds from the seeds of the *C. sinensis* plant. By adding SMILES of the compound, computational toxicity can be predicted, and this website requires no login. This ProTox-II program is categorized into five different classes of toxicity such as carcinogenicity, immunotoxicity, cytotoxicity, mutagenicity, and hepatotoxicity. All of the parameters of toxicity are given in the table containing 70 compounds. Twenty-six compounds among 70 compounds exhibited no toxicity.³⁷

2.7.2. Pharmacokinetics and Toxicity Determination by Using pkCSM. In this research, we proposed the pkCSM server for optimization of pharmacokinetic along with toxicity properties of small molecules; this server basically relies on distance graph-based signatures. The cut-off scanning concept is established in this case, where pharmacokinetic and toxicity

properties of molecules are represented. 51 predictors were divided into five major classes, i.e., absorption (seven predictors), distribution (three predictors), metabolism (five predictors), excretion (two predictors), and toxicity (10 predictors). pkCSM was built with a careful selection of data where all of the parameters were mentioned in the platform.⁴⁷

2.8. DFT Analysis of Active Compounds. Active compounds obtained from ADME were then computed by DFT calculations for the optimization process and generation of MEPs by using Gaussian software at the B3LYP function. For this purpose, the 6-311G basis set was selected in the gas phase calculation. The tool of molecular electrostatic potential was applied to the reactivity as well as the polarity of the selected compounds. (E_{HOMO}) is the highest occupied molecular orbital and has the electron-donating ability, and (E_{LUMO}) is the lowest unoccupied molecular orbital observed for electron-accepting ability. Studying the interaction of molecules inside the compound, the frontier molecular orbital is observed for this process.⁴⁸ Values of E_{HOMO} , E_{LUMO} , and $E_{\text{HOMO-LUMO}}$ energy gap determine the stability (S), electron affinity (A.F), and ionization potential (I.P) of the isolated phytochemicals, respectively. The molecule is polarized and active if the value of the energy gap (ΔE), as well as kinetic bioavailability, is low.^{37,48}

3. RESULTS AND DISCUSSION

3.1. 3D-QSAR Modeling on Screened Phytochemicals against a Gene Mutation in Breast Cancer. **3.1.1. Bioactive Conformation Hunt as well as Template Generation.** Prior research on phytochemicals showed valuable results on anticancer activity, but no reports and literature provide evidence for the required computational approach to a gene mutation in breast cancer. Therefore, the 3D-QSAR technique, also known as the molecular field-based approach, was performed on a series of screened phytochemicals from the plant of *C. sinensis*. Compounds were screened from the library, and a conformational hunt was done for the screened anti-

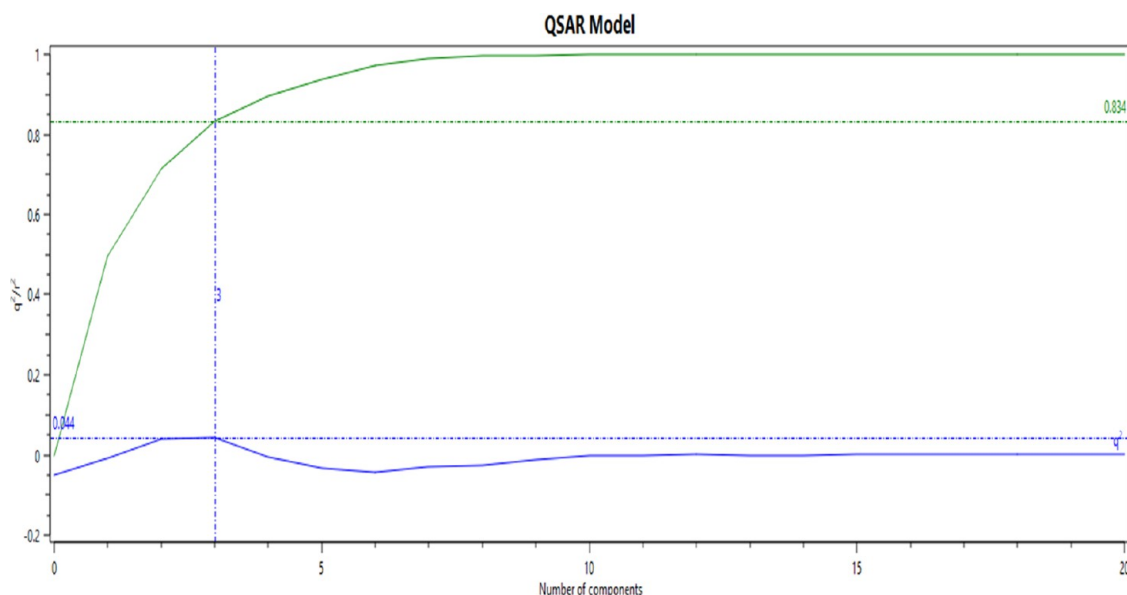


Figure 4. Graph of regression and cross-validation.

breast cancer compounds. The protein (PDB ID: 3EQM) was used in targeting breast cancer caused by gene mutation, and their pharmacophore template was generated. 3D field points were identified after the bioactive conformation of compounds, along with calculating field points. Four types of molecular fields were observed, i.e., van der Waals, positive, and negative, as well as hydrophobicity descriptors. The generated pharmacophore template was used to resemble the required bioactive conformation for virtual screening of the anti-breast cancer compounds, and the molecular field-based approach was applied for this purpose (Figure 3).³⁸

3.1.2. Alignment of Compounds in the Training Set and the 3D-QSAR Approach. Compounds that were present in the training set tended to be aligned to the pharmacophore template, and the alignment of 50 compounds was done. For the development of the model, the biological activity (IC_{50}) of 50 compounds was converted to pIC_{50} using the formula $pIC_{50} = -\log(IC_{50})$. The CSV file of all of the selected 50 compounds was exported to Flare's sheet, where alignment was done normally. Field points were also applied after the alignment of compounds. The data set of 40 compounds was present in the training set, while only 10 compounds were in the test set, and Alpelisib was taken as a reference drug, which was an FDA-approved drug. A partial least-squares (PLS) regression model was obtained, providing regression coefficient $r^2 = 0.80$ and cross-validation $q^2 = 0.567$ values, as shown in Figure 4.

The 3D-QSAR model also showed the difference between the predicted and experimental activities of the compounds. This graph analysis specifies the reliability of QSAR model development, and it also helps in displaying plots of both experimental and predicted values. It is important to note that a cross-validation data point was also obtained along with the plot. Development of the required 3D-QSAR model gives very reliable results by predicting the anti-breast cancer potential of screened phytochemicals. Table 2 illustrates the screened compounds obtained through the 3D-QSAR model.⁴⁹

Alignment was done for all of the screened compounds on the 3D-QSAR model, so according to all of the parameters,

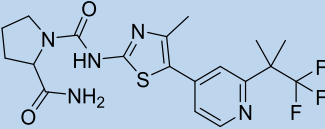
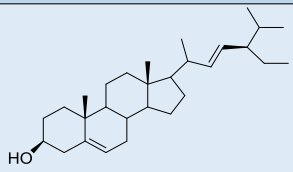
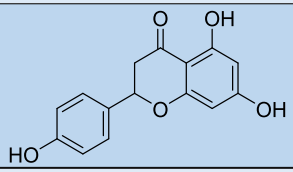
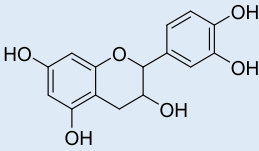
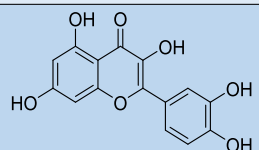
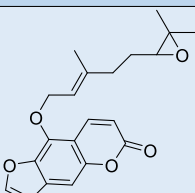
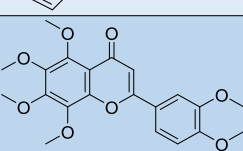
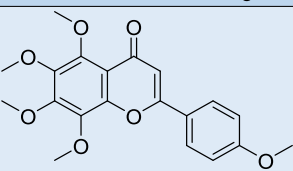
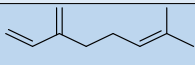
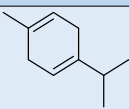
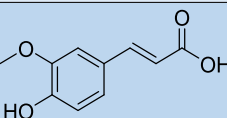
active ligands were selected, and the computed view of aligned active compounds as antagonists is shown in Figure 5.

3.2. SAR Mechanism of Anti-Breast Cancer Compounds by Field Point Regulation. **3.2.1. Identification of Coefficient and Variance Field Points in Anticancer Compounds.** After elucidation of the SAR mechanism of the anti-breast cancer compounds, the visualization (in 3D form) was done for the compounds through the QSAR technique. Different fields generated in the anti-breast cancer compounds such as variance along with coefficients were also analyzed in the 3D form. Furthermore, the localization of the field points of the selected compounds was also compared with the reference drug, i.e., Alpelisib. Coefficient field points as well as variance were obtained and considered as the essential correlating factors in the 3D-QSAR model. The obtained electrostatic effect of the compounds was represented by the large size with cyan and red colors, according to the results. These results indicate that there is a minor role of electrostatic effects in modulating the required activity because of the small size of having pink and green field points in Figure 6. This 3D-QSAR approach was well explained by the resulting electrostatic effects of the compounds.⁵⁴

3.2.2. Field Contributions in Predicting the Activity. Required field contributions were shown by a square in blue color, a triangle in purple color, and a circle in red color geometries, while the area of anticancer compounds in the circle indicates the region of electrostatic field points, along with the capability of the negative regulation based on the predicted activity of compounds. Besides, steric and electrostatics points were indicated by an area of triangle and square having the capability of positive regulation on the predicted activity of anti-breast cancer compounds (Figure 7).⁴⁹

3.2.3. Identification of SAR Mechanisms by Activity Atlas Visualization. The activity atlas approach was applied for further optimization of the anti-breast cancer antagonists as well as for designing new drugs in the pharmaceutical industry. For this purpose, an activity cliff summary and an average of actives were used for anti-breast cancer compounds. The positive field regions were indicated by the red color region enclosing the compounds, whereas red color sites displayed the

Table 2. List of the Screened Compounds as Active Obtained by the 3D-QSAR Approach^{50–515253}

Active compound	Structure	IC ₅₀	Predicted IC ₅₀	Reference
Alpelisib (Reference drug)		10 μM	5	[50]
P8		0.1623 μM	0.266	[51]
P10		0.24 μM	0.287	[51]
P23		0.8 μM	0.321	[51]
P25		0.5 μM	0.262	[51]
P28		0.37 μM	0.293	[19, 52]
P29		0.4 μM	0.2	[19, 52]
P31		0.8 μM	0.219	[19, 52]
P36		0.02 μM	0.361	[19, 52]
P40		0.76 μM	0.304	[19, 52]
P46		0.52 μM	0.32	[53]

higher anticancer potential of compounds. The hydrophobicity of compounds was represented by yellow color, while the average shape of actives was represented by white color, according to results obtained by the 3D-QSAR model.

Favorable and unfavorable regions are also indicated by green and purple colors through this model, respectively. Furthermore, the red color shows no strong structure–activity relationship region of the compounds. It was further revealed

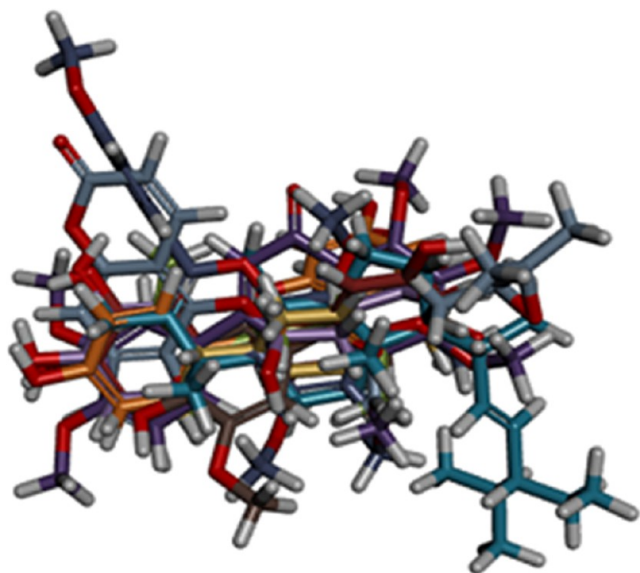


Figure 5. Computed view of aligned active compounds.

through this model that sites of red and cyan colors represent the regions of positive and negative electrostatic fields, and they also correlate with the anti-breast cancer potential of compounds in such a way that if these regions were higher in red or cyan color, then higher anti-breast cancer potential would be indicated. On the contrary, favorable in green color and unfavorable in purple color show hydrophobicity in regulating the anti-breast cancer potential of the compounds as antagonists, as shown in Figure 8.⁵⁵

3.2.4. Validation of the Activity Prediction Model. The compounds that were present in the test and training sets were analyzed for predicting the anti-breast cancer activity by the derived model, and then the error (distance value) was compared as well as determined. The molecular characteristics of the active compounds (as anti-breast cancer agents) were

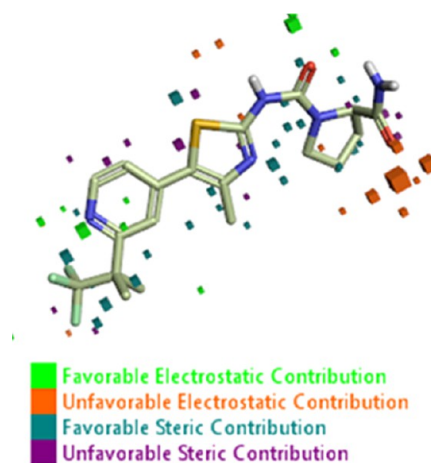


Figure 7. View field contributions to the predicted activity.

retrieved for further prediction of anti-breast cancer potential based on the derived SAR model. When the distance and predicted activity were compared, columns of the models were examined for each model that was derived. This study illustrated the ligand fields for each derived model, and then virtual screening was used for these characteristics.⁴⁹

3.3. Exploring the Anti-Breast Cancer Activity of Phytochemicals Using the In Silico Approach. Docking was performed by using Molegro software on targeted compounds obtained from the 3D-QSAR approach, namely, P8, P10, P23, P25, P28, P29, P31, P36, P40, and P46 as anti-breast cancer agents. MVD helps predict the MolDock score of every ligand and detects various binding sites through the algorithm of cavity detection by creating surfaces and detecting cavities. Favorable poses were also obtained by the MVD software of the active ligands. MolDock scores of selected ligands in this research range from -60.00 to -180.00 after the docking procedure from MVD, while most of the ligands have greater MolDock scores than the reference compound.

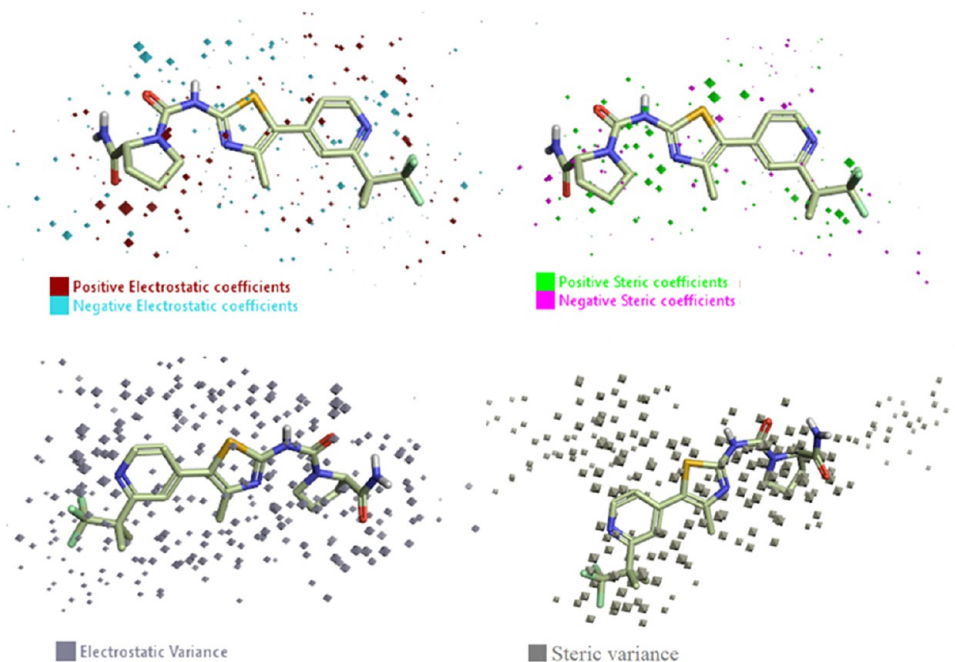


Figure 6. Coefficients as well as variance of the compounds.

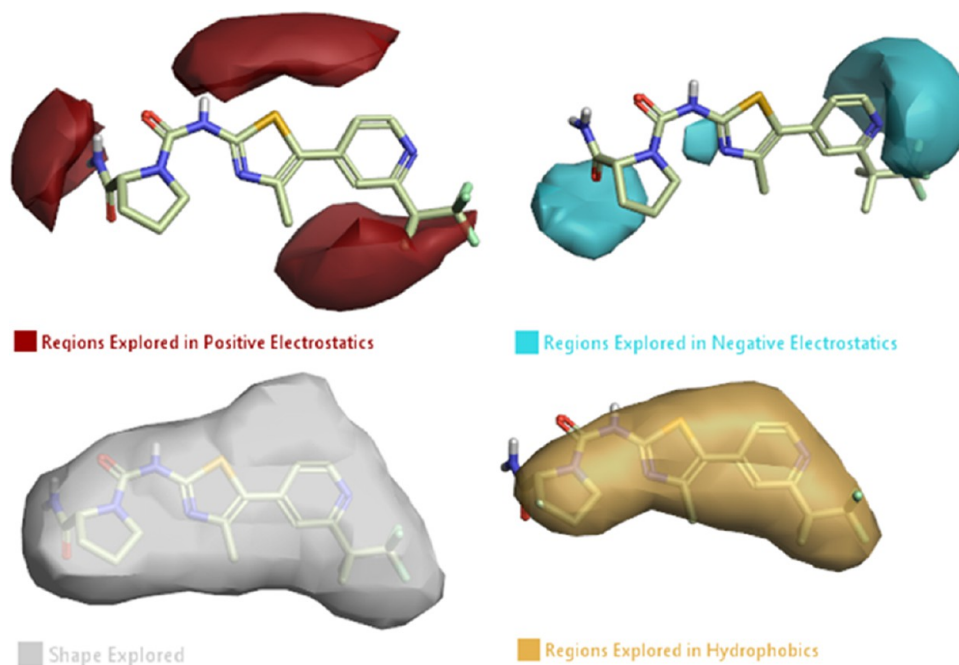


Figure 8. Region explored in positive and negative electrostatics along with hydrophobicity and shape exploration.

Proteins selected for docking studies for BRCA1 were PDB ID: 1T15, 3PXD, 4OFB, 7JZV, and 1T29, while for BRCA2 were PDB ID: 3EU7 and 1IYJ, as shown in Table 4. All of the results of docking analysis as dock score, interactions, and amino acid residues are shown in Table 3 (Zarren et al., 2021).

Ligands with different proteins were visualized and the ligands showed the highest as well as lowest MolDock scores than the reference compound. The compound that showed a higher MolDock score than the reference drug was considered a hit compound.⁴² The MolDock score⁵⁶ of compound **P28** (epoxybergamottin) was -121.625 when docked with 1T15 and was the highest score compared to the other ligands and reference drugs. Compound **P28** showed four hydrogen bonding interactions with GLN1779, THR1700, LYS1702, and ASN1774 amino residues along with eight van der Waals forces, while the reference drug has a MolDock score of -106.294 along with six hydrogen bonds, six van der Waals forces, and one halogen bond, as shown in Figure 9 and Table 3 (Figure S1 in the Supporting Information).

While interacting with 3EU7, another compound that is **P28** also has the highest MolDock score, i.e., -135.797 , than the reference compound and other ligands except for compound **P8**. Compound **P28** has three hydrogen bonding interactions with CYS933, VAL932, and VAL925 amino acid residues along with six van der Waals forces (Figure 10, Table 3, and Figure S2 in the Supporting Information).

Compound **P28** had the lowest MolDock score of -67.3027 when interacting with the 1IYJ protein against gene mutation in breast cancer during Molegro studies when compared with other ligands and reference drugs, but it showed no ligand interactions, as shown in Figure S3 (Supporting Information) and Table 3. Similarly, the reference also did not show any interaction with 1IYJ, and its MolDock score was -50.753 . Compound **P28** achieved the greatest MolDock score of -148.145 when interacting with 1T29, along with three hydrogen bonds with GLY1820, PHE1821, and PRO1771 amino residues as well as 16 van der Waals forces (Figure S4 in the Supporting Information), while the reference compound

had a low score (-133.239) than compound **P28** with seven hydrogen bonds and no van der Waals forces, as shown in Figure S5 (Supporting Information) and Table 3. Compound **P8** had the highest MolDock score, which was -139.997 when docked with the 3EU7 protein, while the reference compound and other ligands had the lowest MolDock score compared to compound **P8**. Compound **P8** has one hydrogen bonding interaction with the ASP1122 amino acid residue, while the reference drug has a MolDock score of -132.956 with four hydrogen bonding and six van der Waals forces, as shown in Figures S6 and S2 (Supporting Information) and Table 3. When the R and S structures of compound **P8** were docked with the 3EU7 protein through Molegro, no difference was observed on the basis of its isomers, as shown in Figures S7 and S8 (Supporting Information).

Compound **P29** when interacting with 3EU7 also had the highest MolDock score of -134.409 compared to the reference drug and other ligands, except for compounds **P8** and **P28**. Compound **P8** showed the highest MolDock score, which was -139.997 , so overall, compound **P8** had the highest MolDock score compared to other ligands when docking was carried out with the 3EU7 protein against gene mutation in the case of breast cancer. Compound **P29** had 10 hydrogen bond interactions and 17 van der Waals forces (Figure S9 in the Supporting Information and Table 3), while the reference drug had 4 hydrogens and 7 van der Waals forces.

3.4. NMA-Based Analysis. A normal mode simulation was performed through the IMOD server (<https://imods.iqfr.csic.es/>) to assess the stability as well as physical movement of protein–ligand complexes. The iMODS server is an online tool used for the analysis of protein flexibility that is based on normal mode analysis (NMA), associated with the coordination of protein–ligand complexes with the docking procedure.⁵⁷ Users can get a friendly interface of the IMOD server for the NMA function, which helps in exploring 3D structures along with the simulation of suitable trajectories between two or more conformations for smaller as well as larger molecules. This type of tool is very beneficial in providing structural

Table 3. Compounds with the Best MolDock Scores

compound	protein	MolDock score	amino acid residues	type of interaction	distance		
alpelisib	1T15	−106.294	ILE1618	conventional H-bond	2.70732		
			THR177	conventional H-bond	3.0484		
			LEU1701	conventional H-bond	2.46828		
			LYS1702	conventional H-bond	1.60974		
			GLN1779	conventional H-bond	2.79257		
			ASN1774	conventional H-bond	1.63785		
			ILE1680	halogen (fluorine)	3.21767		
			LEU1679	alkyl	4.17668		
			LEU1679	alkyl	3.27215		
			LEU1679	alkyl	4.09315		
			PRO1776	alkyl	4.08091		
			PRO1776	π -alkyl	4.01189		
			PRO1776	π -alkyl	4.44967		
			3EU7	−132.956	SER873	conventional H-bond	2.52658
	ALA874	conventional H-bond			1.8306		
	ASP927	conventional H-bond			1.9135		
	VAL928	carbon H-bond			2.26297		
	PRO924	π -sigma			2.14349		
	PRO924	alkyl			5.03458		
	PRO926	alkyl			4.37738		
	MET874	alkyl			3.44898		
	PRO926	alkyl			4.78296		
	MET875	π -alkyl			4.66629		
	PRO926	π -alkyl			5.33599		
	1IJY	−50.753				no ligand interactions	
	1T29	−133.239			GLY1820	conventional H-bond	1.73596
	stigmasterol (P8)	3EU7			−139.997	PHE1821	conventional H-bond
			HIS1822	conventional H-bond		2.28367	
ASP1818			conventional H-bond	1.90818			
ASN1819			conventional H-bond	1.85315			
THR1816			carbon H-bond	2.86507			
PRO1812			carbon H-bond	2.35261			
ASP1122			conventional H-bond	1.82696			
PRO924			alkyl	4.97265			
PRO926			alkyl	4.93081			
LYS1124			alkyl	5.09845			
LYS1124			alkyl	5.03004			
MET875			alkyl	4.29053			
MET875			alkyl	4.3956			
VAL925			alkyl	4.70734			
MET875			alkyl	3.09277			
PRO924			alkyl	4.7717			
TYR929			π -alkyl	4.56328			
epoxybergamottin (P28)			1T15	−121.625		GLN1779	conventional H-bond
	THR1700	carbon H-bond			2.27478		
	LYS1702	carbon H-bond			2.55299		
	ASN1774	carbon H-bond			2.37728		
	LIG1	π -sigma			2.79742		
	PRO1776	alkyl			5.46091		
	LEU1701	alkyl			4.95755		
	LEU1679	alkyl			3.60579		
	ILE1680	alkyl			5.35979		
	PRO1776	alkyl			4.08603		
	LEU1701	π -alkyl			4.34125		
	LEU1701	π -alkyl			4.73257		
	3EU7	−135.797			CYS933	conventional H-bond	1.7397
					VAL932	carbon H-bond	2.11917
			VAL925	π -donor H-bond	2.58575		
			MET875	π -sulfur	3.80498		
			LYS1124	alkyl	3.81758		
			PRO924	alkyl	3.74815		

Table 3. continued

compound	protein	MolDock score	amino acid residues	type of interaction	distance	
nobiletin (P29)	1IJY 1T29	−67.3027 −148.145	MET875	π -alkyl	5.02535	
			PRO924	π -alkyl	4.39419	
			MET875	π -alkyl	3.89296	
			PRO924	π -alkyl	4.93723	
					no ligand interactions	
				GLY1820	conventional H-bond	2.91427
				PHE1821	conventional H-bond	2.15518
				PRO1771	carbon H-bond	2.14344
				PHE1821	π -sigma	1.89751
				PHE1821	π - π stacked	4.76445
				HIS1822	π - π T-shaped	5.86284
				VAL1810	alkyl	3.84944
				PRO1812	alkyl	4.01619
				ALA1814	alkyl	4.4717
				PRO1771	alkyl	4.19017
				VAL1810	alkyl	3.97908
				PRO1771	alkyl	5.07658
				VAL1810	alkyl	3.34444
				VAL1810	alkyl	5.39536
				PRO1812	alkyl	3.01682
				ILE1855	alkyl	4.01817
				TYR1769	π -alkyl	5.33257
				PHE1772	π -alkyl	4.4545
				PHE1821	π -alkyl	3.87055
		3EU7	−134.409	CYS933	conventional H-bond	1.86056
				VAL932	carbon H-bond	2.38969
				LIG1	carbon H-bond	3.02891
				TYR929	carbon H-bond	2.6645
				LIG1	carbon H-bond	2.30752
				ASP927	carbon H-bond	2.33961
				LIG1	carbon H-bond	2.47632
				LIG1 LEU931	carbon H-bond	2.45015
				VAL925	carbon H-bond	2.48905
			PRO926	π -donor H-bond	2.87686	
			MET875	π -sigma	2.12324	
			MET875	π -sulfur	5.82108	
			VAL925	π -sulfur	3.71688	
			VAL925	amide- π stacked	3.71058	
			PRO924	amide- π stacked	4.16172	
			PRO926	alkyl	4.36439	
			VAL925	alkyl	4.65723	
			VAL928	alkyl	3.81973	
			LEU931	alkyl	4.61942	
			CYC933	alkyl	5.03197	
			MET875	alkyl	4.69339	
			ILE888	alkyl	5.00695	
			ILE922	alkyl	3.5708	
			VAL932	alkyl	3.78955	
			PHE876	alkyl	3.06638	
			TYR929	π -alkyl	4.82143	
			PRO926	π -alkyl	5.04096	
			PRO924	π -alkyl	5.29185	
				π -alkyl	4.28328	

mobility of compounds that have been docked based on the NMA study.⁵⁸ Two important factors have been determined by this interface: one is deformability, which shows the flexibility of the protein, and the other factor is the B factor, which shows the mobility of the protein. A graph of deformability was obtained, which showed that different multiple peaks had a

range close to 1.0. In this research, the compound P28 with 1T29 complex has shown maximum flexibility at 1.0, which is the highest peak with high deformability, while the graph of the B factor explained the comparison of PDB and NMA studies (Figure 11A). Both deformability and B factor plots helped in displaying the comparison of PDB fields along with the NMA

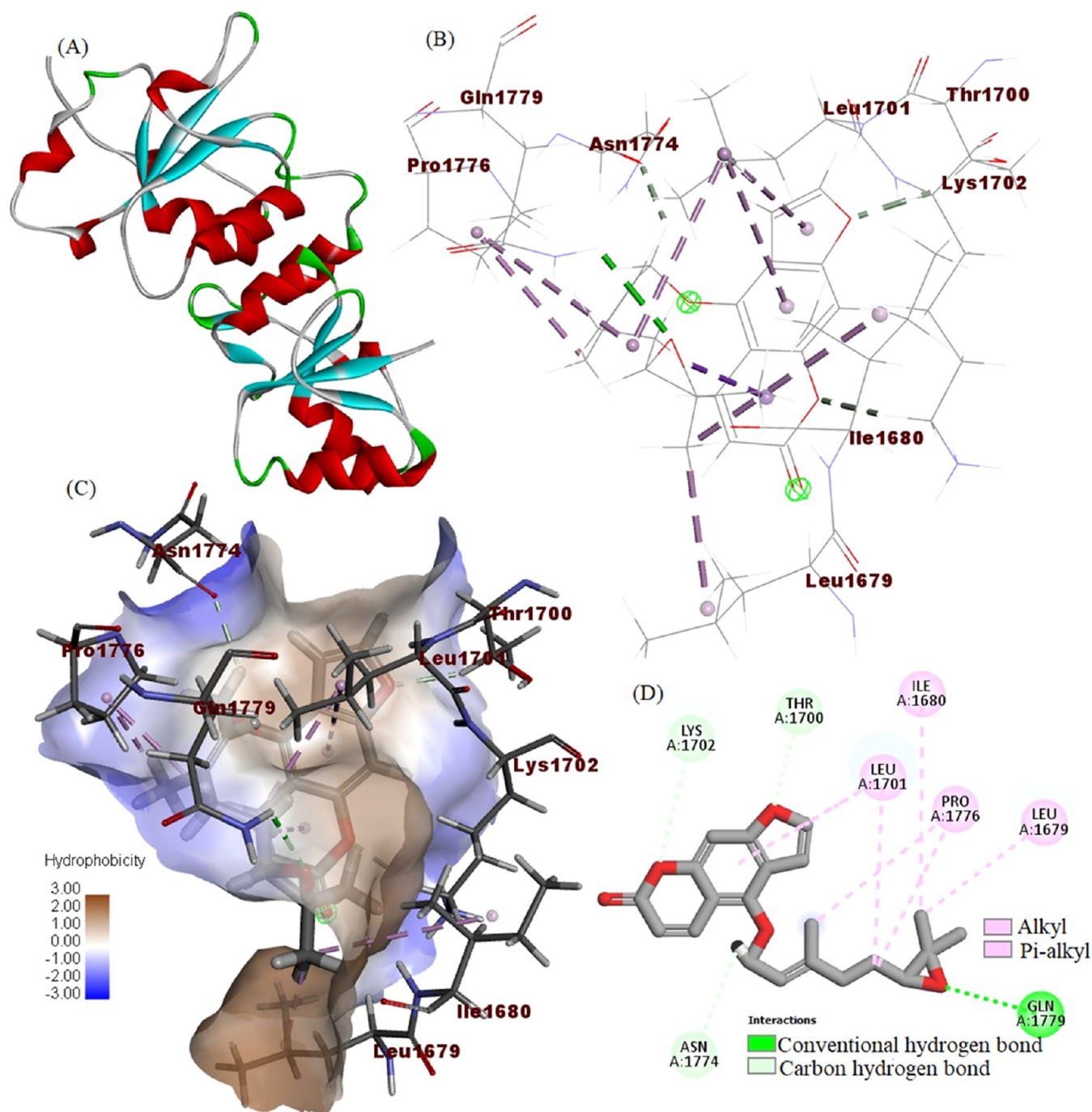


Figure 9. Epoxybergamottin (28)–protein–ligand interaction with 1T15 along with hydrophobicity and 2D structure.

studies. Figure 11B shows that eigenvalues along with variance are inversely linked with each other. A compound with a low eigenvalue was considered to be more effective in the MD simulation procedure because minimum energy would be used, and in this way, deformability would become easy for respective structures. Compound P28 has achieved a low eigenvalue, as shown in Table 4, whereas the variance plot showed bars of purple color for isolated variance, while cumulative variance is indicated by green color bars shown in Figure 11B.

Figure 12C,D shows a plot of the elastic network model and a covariance plot. The docked proteins were displayed in the elastic network model, which represents a stiffer portion of the

protein in the dark gray region of the plot. The correlation was indicated during the MD simulation between residues of the compounds through a covariance plot. The red color indicates a strong correlation between residues and is considered the better complex, while the blue color showed anticorrelations, and the region in white color showed the uncorrelated motion of the complex.⁵⁹

For output results, RMSF is an important factor in MD simulations; higher flexibility is indicated at maximum peaks, resulting in more fluctuation, and the motion of the molecular structure was restricted at a lower value in the plot.⁵⁸ The maximum peak obtained for the complex after MD simulations was 1.000 Å at 128 residues, while a minimum of 0.159 Å at 75

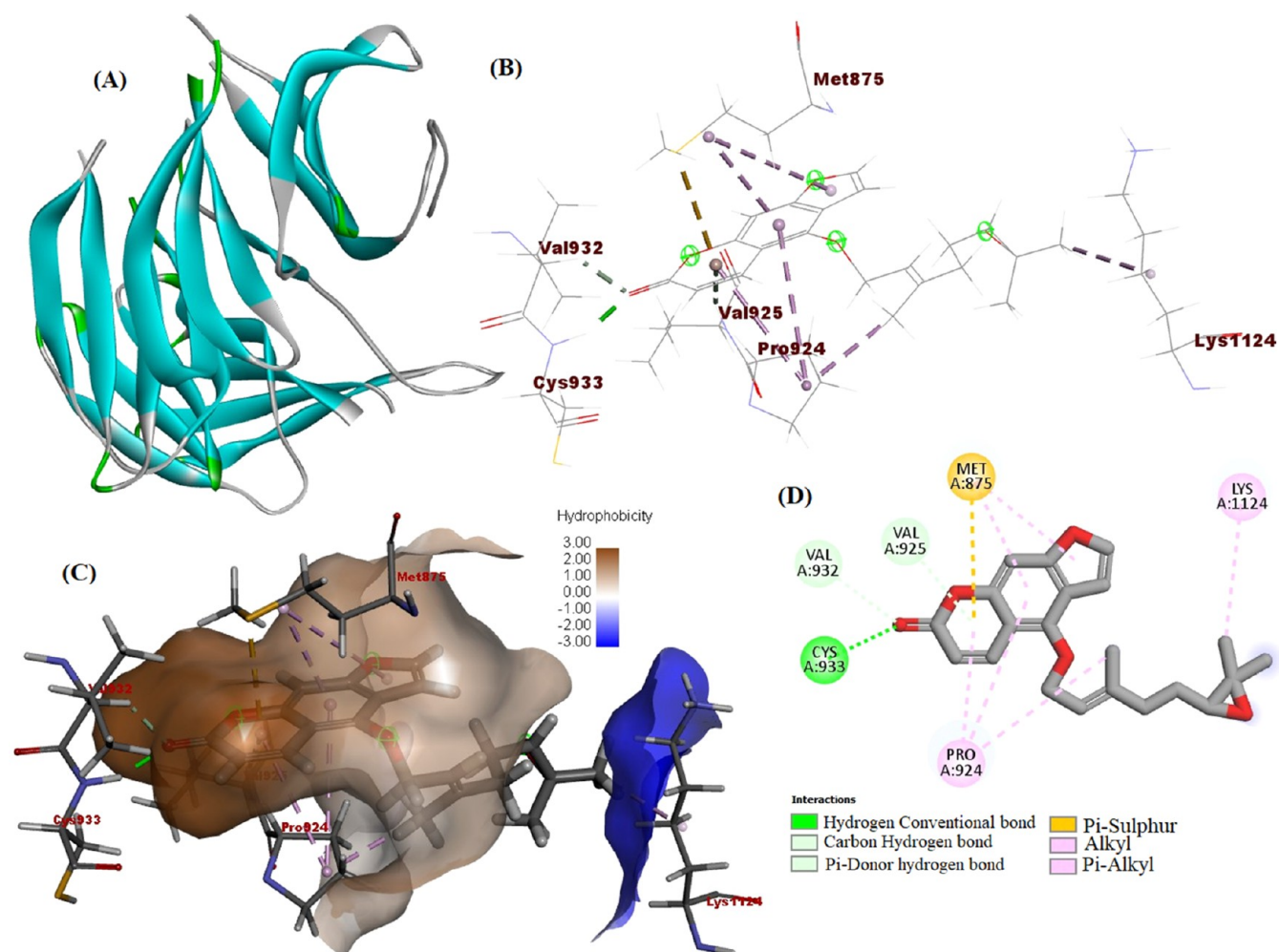


Figure 10. (A) Protein; (B) epoxybergamottin protein–ligand interaction with 3EU7; (C) hydrophobicity; and (D) 2D structure.

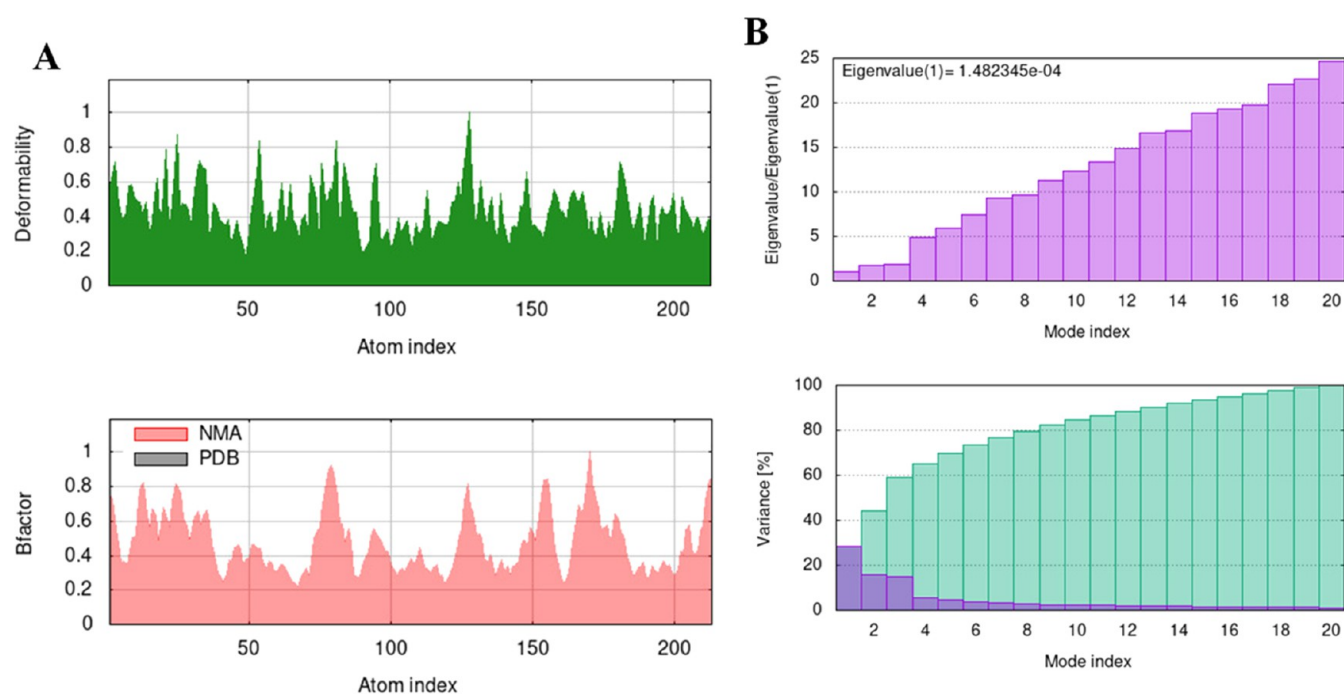


Figure 11. (A) Plot of deformability along with B factor and (B) plot of eigenvalue and variance for the P28–1T29 complex.

Table 4. Eigenvalues of Complexes

complex	eigenvalues of complexes
1T29	1.482345e-04
1T15	1.492457e-04
3EU7	6.128068e-05

was obtained, as shown in Figure 13E. The P28–1T15 complex showed mobility profiles through deformability in which the peak was observed at the highest value of 1.0, which is considered a high deformability region. The comparison of PDB fields and NMA studies is shown by the B factor plot in Figure 13A. A lower eigenvalue is also obtained through the plot shown in Table 4, while variance is shown in Figure 13B.⁵⁸

An elastic map along with a covariance plot is also obtained and shown in Figure 14C,D. The complex showed a maximum peak at 1.000 Å at 128 residues, while a minimum of 0.165 Å at 49 was obtained during MD simulations, as shown in Figure 14E.

The compound P28 with 3EU7 complex shows deformability of around 1.0, and a comparison between the PDB field along with the NMA study is illustrated in Figure 15A. The eigenvalues of this complex obtained were very high, as shown in Table 4. Therefore, more energy would be required for the

deformability of the structure, and this complex was not considered a better one, as shown in Figure 15B. The elastic map and covariance plot are obtained in Figure 16C,D.⁶⁰

The maximum peak of the resulting complex obtained was at 1.000 Å at 2 residues with multiple peaks, while a minimum of 0.0359 Å at 140 was obtained after the MD simulation task, as shown in Figure 16.

3.4.1. Root-Mean-Square Deviation (RMSD), Radius of Gyration, and Protein–Ligand Contact Plot of the 1T29 Protein. Lead protein 1T29 was obtained after MD simulations, and then for the stability purpose of the protein structure in all simulations, the RMSD (Figure S10 in the Supporting Information) and radius of gyration (Figure S11 in the Supporting Information) of two chains, i.e., A and B of the protein, were calculated from the iMODS server. The protein–ligand contact plot (time vs RMSD) was also obtained, as shown in Figure S12 (Supporting Information). At every iteration, the α -RMSD is computed. Final RMSD values are around 1 or 2 Å. Lead protein 1T29 has shown the RMSD value of 1.64, which is acceptable according to standard <https://imods.iqfr.csic.es/>.⁶¹

3.4.2. Molecular Dynamics Simulation. The MD simulation was performed for the complexes that were generated

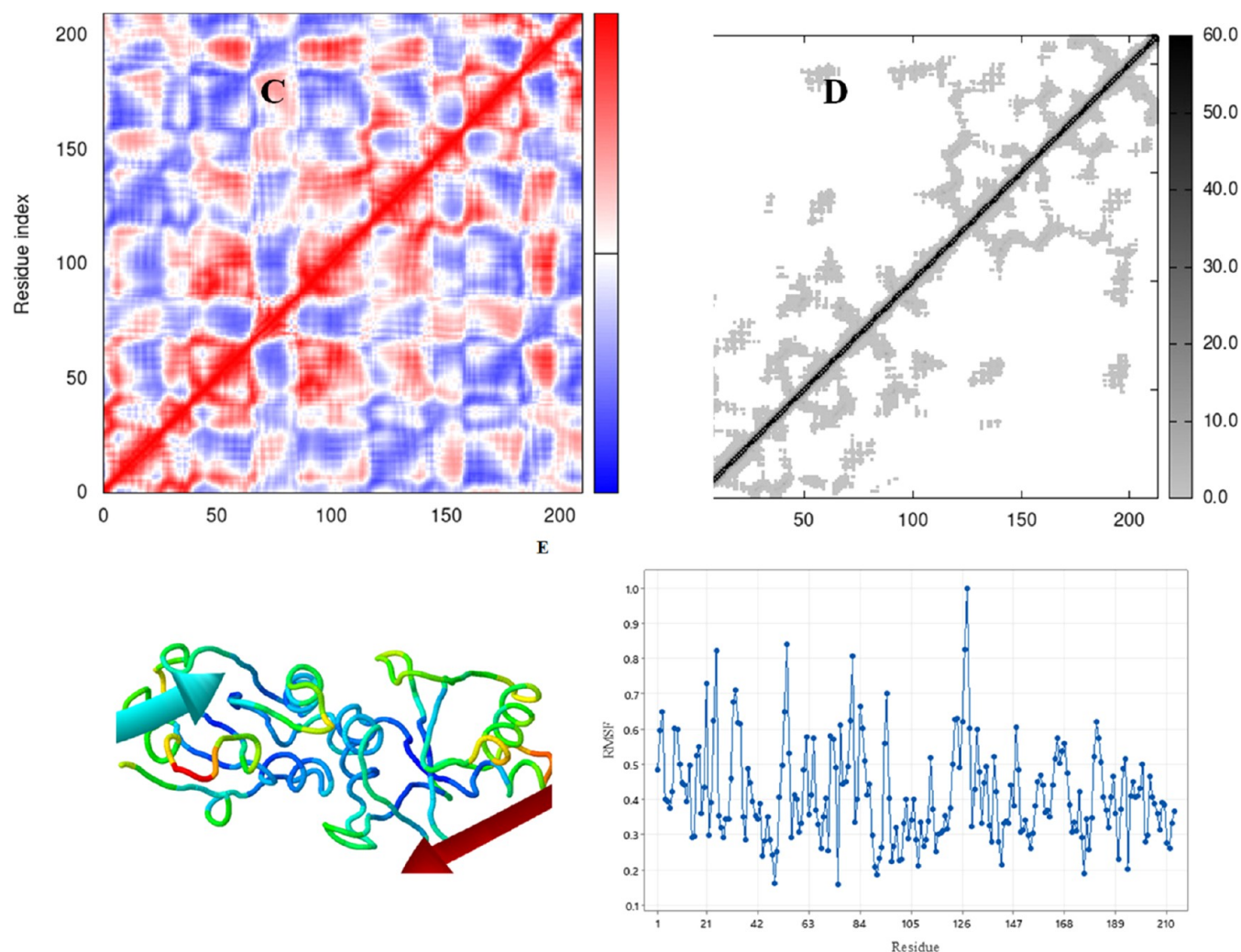
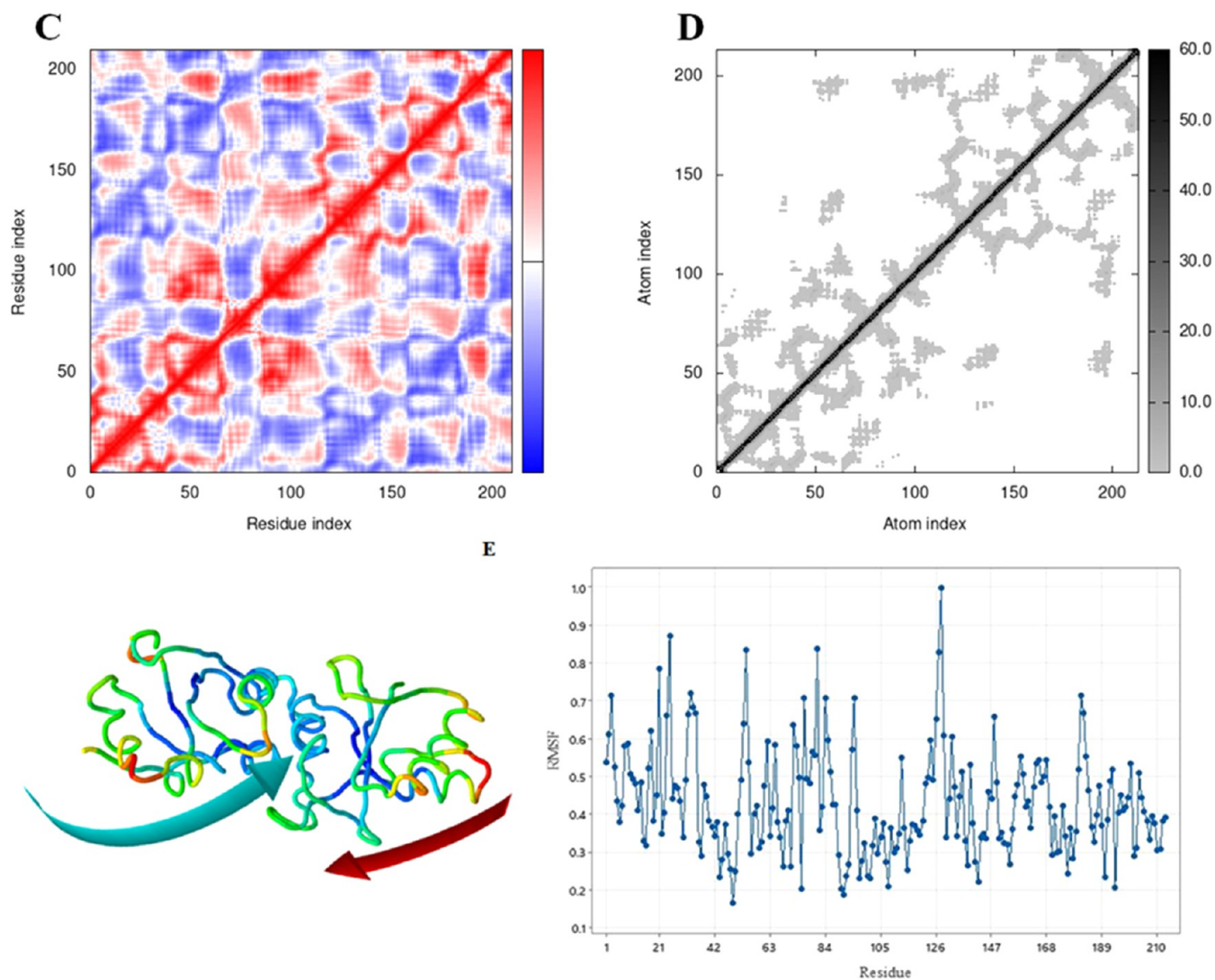
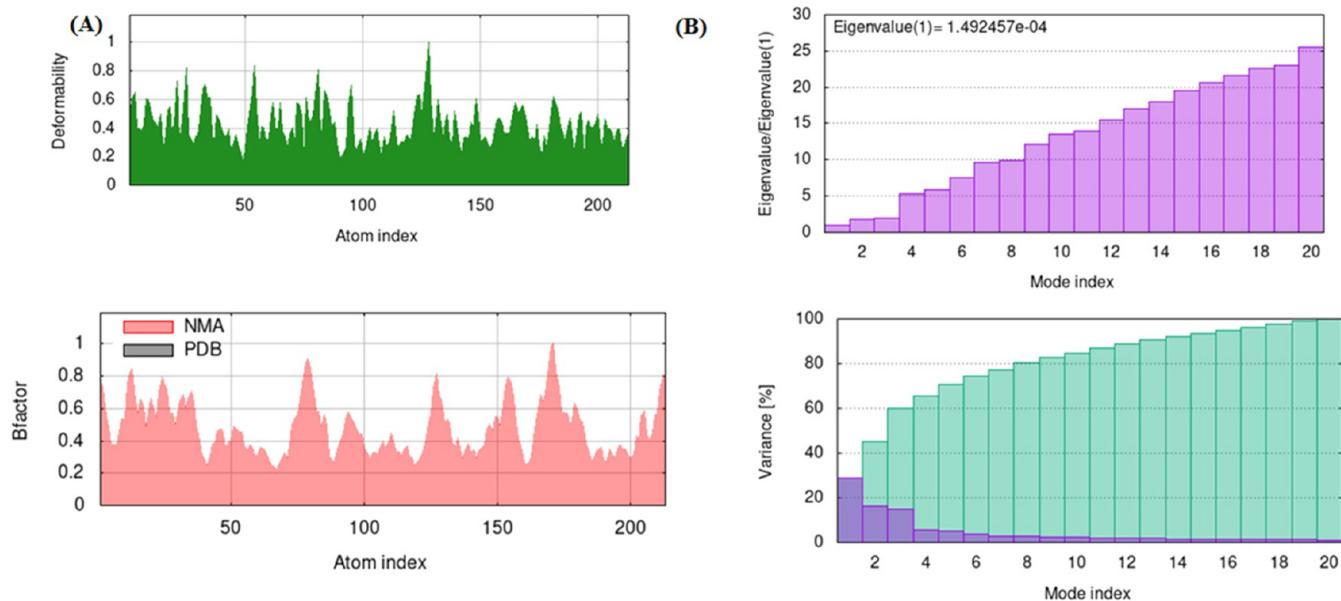


Figure 12. Elastic network model (C) and covariance map (D) for P28–1T29. (E) Root-mean-square fluctuation (RMSF) value for the P28–1T29 complex.



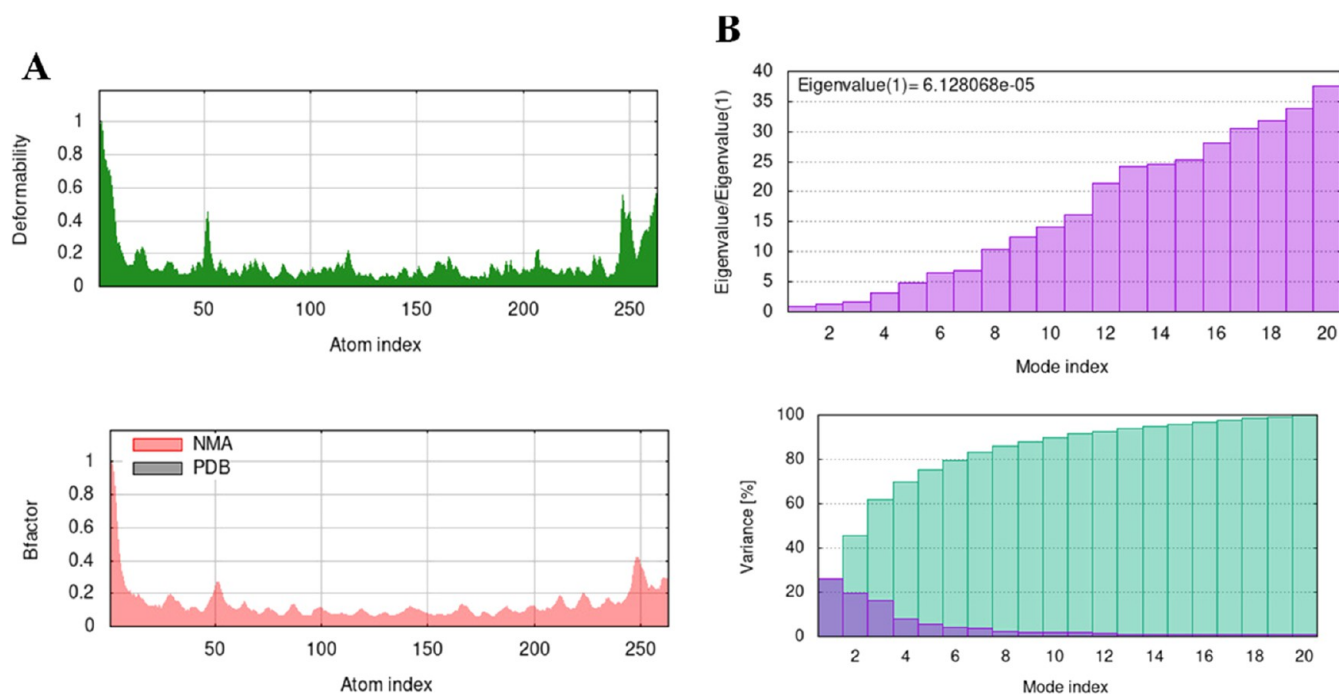


Figure 15. Deformability and B factor (A) and eigenvalue and variance (B) for the P28–3EU7 complex.

through docking studies in order to establish the most effective binding site of the compound. After completion of 100 ns run time, RMSD was evaluated, which helped in assessing the stability of selected complexes, and in this way, a strong interaction of the ligand with the binding site was evaluated.⁶²

At 100 ns, P28–1T15 showed an RMSD of 0.9–1.5 Å, represented by the gray color in the graph, P28–1T29 showed an RMSD of 0.8–1.9 Å, represented by blue curves in the graph, and P28–3EU7 showed an RMSD of 1.0–2.3 Å, represented by red curves in the graph. All of the protein–ligand complexes have good RMSD values, but P28–1T15 dominated all of them due to the lowest RMSD value, leading to great stability. At 100 ns, the RMSF of the complexes showed the minimum and maximum fluctuations at the specific amino acid residues. P28–1T15 had minimum fluctuation at residue number 20 and maximum fluctuation at residue number 150, P28–1T29 showed minimum fluctuation at residue number 25 and maximum fluctuation at residue number 140, and P28–3EU7 showed minimum fluctuation at residue number 27 and maximum fluctuation at residue number 225 (Figure 17).

The compatibility of all of the complexes was determined by plotting the Rg and Hb graphs. Out of all of them, complex P28–1T15 shows stable Rg and Hb graphs at a time scale of 100 ns as compared to two other complexes (shown in Figure 18).

As shown in Figure 19, all of the complexes had good electronic energy, but complex P28–1T15 was found to dominate all of the complexes due to its electronic energy of -2.750 , which is more stable than other complexes. MD simulation results validated the molecular docking by confirming the stability of the complex during the simulation process. The leads found in docking were also confirmed by MD simulations.

3.4.3. MM-GBSA. The MM-GBSA calculation method is primarily used for rescoring the docked pose of the ligand. These poses are taken as inputs for energy minimization for

the protein–ligand complexes. It generates different ligand orientations by using various docking software, which further employ it for starting ligand–receptor coordinates for MD simulation analysis. Ligand protein interactions and the reliability of the computational drug discovery process should be considered for a comprehensive study.⁶³ The binding affinity of the protein with compound P29 when compared with the reference drug alpelisib through MM-GBSA has a higher negative value for binding energy, as shown in Table 5. This value indicates a strong affinity to proteins and ligands.⁶⁴

3.5. ADME Studies of Anticancer Compounds. This study provides researchers with quantitative information about the disposition of a drug. ADME/Tox and pharmacological properties play significant roles in clinical success. The tool used for analyzing the process of ADME is SwissADME.⁶⁵ For the determination of the drug ability of the molecule, the rule, i.e., Lipinski's rule of five, is used for this purpose. Another drug-likeness rule includes Ghose, Veber, Egan, and Muegge. For a perfect drug designing process, this rule includes various restrictions such as there should be only one violation for orally active drugs, hydrogen bond donors (N and O having hydrogen atoms), as well as acceptors (all nitrogen or oxygen atoms), should not exceed more than 5, the molecular weight of the drug should be less than 100 g/mol because small-sized drugs are more valuable, and moderately lipophilic molecules. Tables S2 and S3 in the Supporting Information show compounds obtained after the ADME study.⁶⁵ The results obtained were found in good agreement to prove that the *Citrus sinensis* compounds are safe and drug-like for use; 26 compounds among 70 compounds exhibited no toxicity (Table S3 in the Supporting Information). The results of all our studies match best with the ADMET results by suggesting the best compounds P28 and P29.

3.5.1. pkCSM analysis. pkCSM was built with a careful selection of data where all of the parameters are mentioned in the platform (Table S4 in the Supporting Information).⁴⁷ Absorption is the movement of the drug to the bloodstream

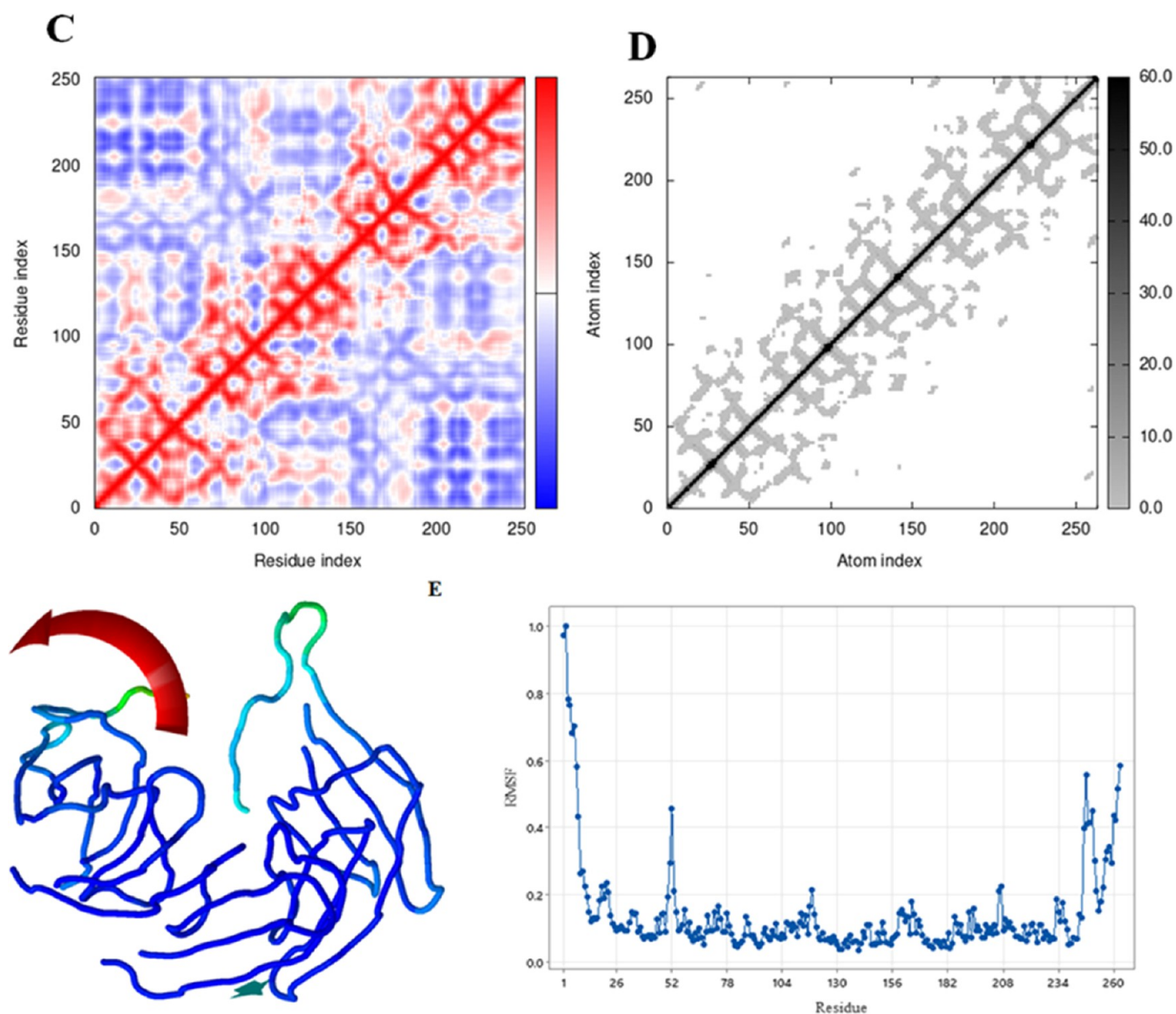


Figure 16. Elastic map (C) and covariance (D) for the P28–3EU7 complex. (E) Maximum and minimum values at residues for the P28–3EU7 complex.

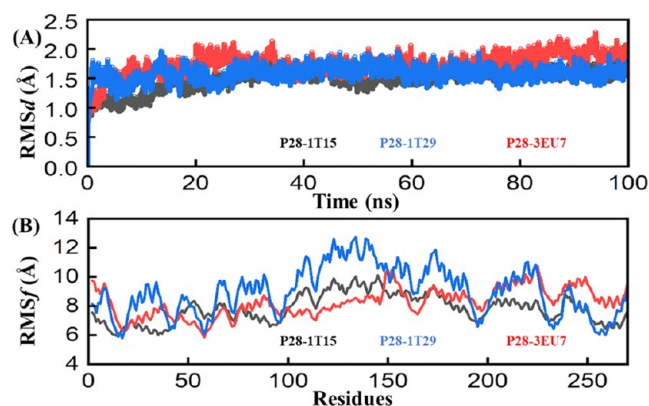


Figure 17. (A) RMSD regarding the complexes P28–IT15 (black line), P28–IT29 (blue line), and P28–3EU7 (red line). (B) RMSF of all residues of P28–IT15 (black line), P28–IT29 (blue line), and P28–3EU7 (red line).

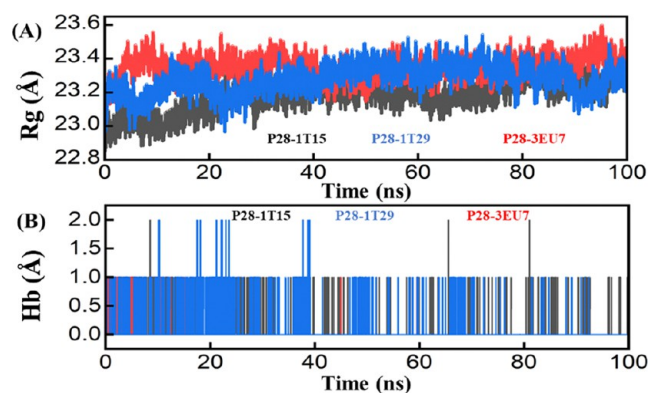


Figure 18. (A) Radius of gyration (R_g) regarding the complexes. (B) Hydrogen bonding (Hb) regarding the complexes.

from the site of administration in the human body. For the acceleration of the absorption process, it is important for a drug to be effectively soluble in aqueous media. But if it is too

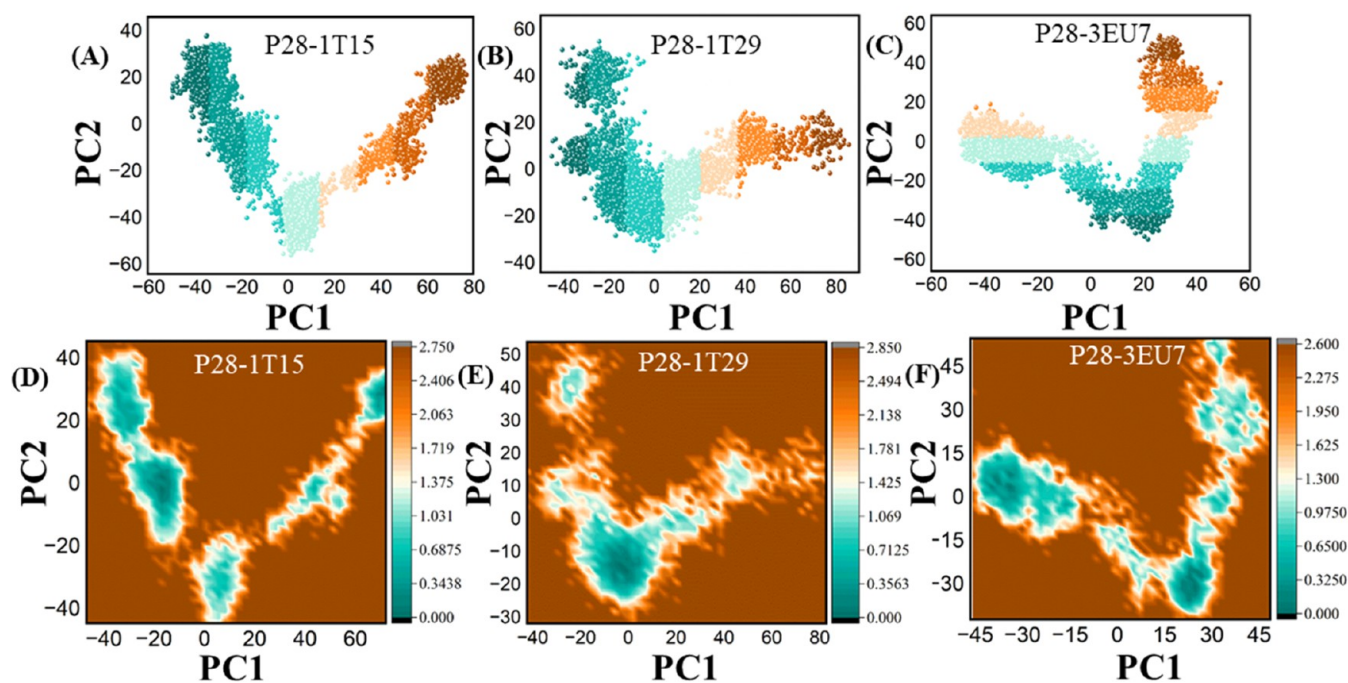


Figure 19. Electronic energy of complexes obtained from MD simulations by principle component analysis.

Table 5. Energy Binding Values

compounds with 1T29 complex	ΔG ligand	ΔG receptor	ΔG complex	ΔG binding = ΔG (complex) - ΔG (receptor) - ΔG (ligand)
alpelisib	2.737	-8609.64	-8687.02	-80.117
compound P8	2.458	-8609.64	-8647.1	-39.918
compound P28	1.985	-8609.64	-8662.99	-55.245
compound P29	3.4	-8609.64	-8719.15	-112.91

soluble, then it will get excreted out from the body without showing any effect. Out of 51 obtained phytochemicals, 37 showed moderate solubility below -5.00 log mol/L, while the other 14 compounds showed within the optimum range of -5.02 to -11.04 log mol/L. The drug could be administered through inhalation, ingestion, or dermal contact, but it should cross the membrane before entering the bloodstream. There are about four ways through which the chemical or drug crosses the membrane and enters the body, such as active diffusion, passive diffusion, facilitated diffusion, and endocytosis. Metabolism is an important chemical process for drug–drug interactions as well as for bioavailability. Enzyme cytochrome p-40 known as membrane-bound hemoprotein is a major site where the drug–drug interaction takes place. Cytochrome p-40 is an enzyme that is important for cellular metabolism as well as for detoxification of xenobiotics. CYP1A2, CYP2A6, CYP2B6, CYP2C8, CYP2C9, CYP2C19, CYP2D6, CYP2E1, CYP3A4, and CYP3A5 are the subfamilies of CYPs in the human body; these enzymes help in metabolic reactions.

Prediction for skin permeability was also calculated for isolated compounds from the seeds of *C. sinensis*, represented as Log Kp (skin permeability coefficient). Less skin permeability of the drug was obtained for a more negative value of log Kp (with Kp in cm/s). Kp values predicted were in the

range from 0.04 to -10.90 cm/s. Excretion for total clearance was in the range of 0.006–0.19, while toxicity has different values. All of the compounds showed AMES toxicity 0, while the maximum tolerance dose ranged from -0.176 to 2.102.⁴⁷

Compounds P28 and P29 have water solubility ranges of -4.803 and -4.949 , respectively. Their skin permeability values are -2.866 and -2.715 , AMES toxicity is 0, and maximum tolerance doses are -0.121 and 0.789, respectively (Supporting Information).

3.6. DFT Analysis of Lead Compounds. Computational studies used as a tool in the design and for the theoretical study of phytochemicals from plant species have been upgraded by the development of a significant technique, i.e., density functional theory (DFT). This technique is considered very simple and valuable for understanding mechanistic issues and computational studies of the structures of atoms, surfaces, crystals, molecules, and their interactions. For analyzing the science of solids and chemistry, this theoretical study is beneficial for analyzing at the molecular level.⁶⁶ The 2D structures of active compounds P28 and P29 were drawn in PerkinElmer ChemDraw and then converted into a 3D structure with the help of Chem 3D. DFT calculation was carried out through Gaussian along with GaussView 06 software to achieve structure optimization of compounds. Moreover, B3LYP and 6-311G were the basis sets selected for the calculations.^{67,66} Dipole moment, electrophilicity index, electronegativity, energy gap, net charge, and electron affinity, as well as ionization potential are shown in Table S5 (Supporting Information). For determining the chemical reaction mechanism, the contour diagrams of HOMO and LUMO were considered important parameters and calculated accurately. Contour diagrams are shown in Figure S14 (Supporting Information). Information about stability, chemical softness, reactivity, and stability can be obtained through frontier molecular orbitals (FMOs). Qualitative information on LUMO susceptibility in accepting the electrons from HOMO can be achieved from HOMO–LUMO analysis. At the basis

sets of B3LYP and 6-311G, HOMO and LUMO energies values of active compounds were measured with the help of the DFT method. All of the calculated energy parameters as well as molecular charge transfer interactions of both active compounds are shown in Table S5 (Supporting Information).

E_{HOMO} is the first computational parameter shown in Table S5 (Supporting Information). A compound is considered a strong electron donor and can donate its electron to an acceptor if values of HOMO are higher, due to which biological activity will be increased.⁶⁶ As a result, increasing E_{HOMO} values of the following compounds are as follows.

Compound P29 > Compound P28

E_{LUMO} is the second computational parameter shown in Table S5 (Supporting Information). If the compound possesses low E_{LUMO} values, then it means that it can accept electrons from the donor molecule. That is why biological activity will be increased with decreased E_{LUMO} values.⁶⁶ According to Table S5 (Supporting Information), the increase in the biological activity of the following compounds is as follows.

Compound P28 > Compound P29

The energy gap (ΔE) is another parameter. According to the values of HOMO as well as LUMO, it is indicated that energy present in the HOMO is more stable than that in the LUMO as well as has a small energy gap. The small gap shows that the molecule is chemically reactive, kinetically unstable, and biologically stable; therefore, a decrease in the energy gap increases the biological activity of the compound, and the ranking is as follows.

Compound P28 > Compound P29

Recent research has reported that values of both orbitals play a significant role in the determination of biological activity as well as stability of drugs. As analyzed by FMO, the compound value of HOMO was higher for compound P29 than compound P28, and it could be the better electron donor according to the studies. Interactions could be shared by HOMO and LUMO with adjacent residues of the drug during the binding process⁶⁶ (Figure S13 in the Supporting Information). The chemical hardness (η) of compound P29 was low, and the chemical softness (S) of compound P29 was found to be higher than compound P28, so compound P29 was confirmed more reactive. The electronegativity (χ) and electrophilicity index (ω) of compound P28 have high values, which means that it has a more attractive ability as compared to compound P29. The chemical potential ($-\chi$) of compound P29 was more than that of compound P28. As both compounds possess negative values, it means that both were reducers in nature, and under specific proteins, both can go under oxidation reactions. HOMO and LUMO analysis is helpful for us in providing quantum chemical parameters such as electrophilicity index, chemical potential, energy gap, electronegativity, and chemical softness along with chemical hardness.⁶⁶ These parameters can be calculated by following the formulas shown in Table S5 (Supporting Information). The chemical potential has a high value, while electronegativity has low values because of electron delocalization, which means that the molecule can coordinate with the biological system easily by forming bonds. According to this criterion, the ranking of the compound was found as follows.

Compound P29 > Compound P28

According to the DFT calculations, compound P28 has a greater value of dipole moment than compound P29, so the order was found as follows.

Compound P28 > Compound P29

Compound P28 has a high value of dipole moment, which means that there is a strong interaction between the protein as well as the ligand through electrostatic attraction, and has the best conductivity as well through the process of oxidation.⁶⁸ For the interpretation of nucleophilic and electrophilic attacks as well as the prediction of hydrogen bonding interactions, MEP was observed as a very helpful technique and was also responsible for determining the chemical mechanism. The reactivity of synthesized drugs against nucleophilic as well as electrophilic attacks can be estimated through the molecular electrostatic potential.⁶⁷ The MEP of both compounds, i.e., P28 and P29, was determined by the same base set through the same process. The electrophilic site is represented by a red and yellow area in the MEP, indicated with a negative charge, meaning that electrophiles can react with oxygen atoms. On the other hand, benzene rings are considered neutral because they show neutral reactivity. Figure S15 (Supporting Information) shows the MEP structure and MEP scale of both active compounds based on SCF energy.⁶⁷

Results of DFT showed that P28 was the best hit because all chemical descriptors of DFT analysis displayed the best results for compound P28. These results of DFT further validate the findings obtained by docking and MD simulations in close agreement.

4. CONCLUSIONS

The conventional study could not provide strong evidence in predicting the toxicity of the compounds because for toxicity prediction, different molecular scaffolds along with a weak affinity for chemicals are considered. Therefore, SAR was developed to facilitate researchers by providing various scaffolds of anti-breast cancer antagonists to the drug discovery industry. For this purpose, multistep SAR models were introduced for screening the antagonists with a combination of different computational methods. In the first screening step, SAR was developed with the help of Flare software, and the most reliable antagonists were obtained. The combinatorial study identified new antagonists (stigmaterol P8, epoxybergamottin P28, nobiletin P29) with comparable potential as antagonists among 10 compounds that were obtained after a flare. The 3D-QSAR model has provided some valuable insights into the molecular interactions and structural features that help facilitate the compounds' activity for anti-breast cancer cells. When these active compounds were analyzed for a structure-based drug design tool, the protein receptor target was also considered. The process of docking through Molegro software has provided the best MolDock score for the hit compounds. MD simulations confirmed epoxybergamottin P28 as a better alternative due to maximum peaks at the required range with more fluctuations, correlations, and flexibility of a protein with compounds because of their intermolecular interactions. ADME prediction results further supported and confirmed epoxybergamottin P28 and nobiletin P29 as the best breast cancer inhibitors as antagonists, clearing all of the factors involved in the computational study. The resulting antagonism was further evidenced by DFT studies, which found that all parameters justified the results. Therefore, these results will be beneficial in the multistep screening process and could become an effective tool in determining reliable antagonists for breast cancer disease. This study also summarizes various advancements in computational drug design that provide awareness of recent drug discoveries in

the future to design a new target. This study identified new candidates for drug development.

■ ASSOCIATED CONTENT

SI Supporting Information

The Supporting Information is available free of charge at <https://pubs.acs.org/doi/10.1021/acsomega.3c05098>.

Phytochemicals obtained from the seeds of the *Citrus sinensis* plant; compounds obtained after ADME prediction; quantum chemical parameters based upon DFT computations at DFT/B3LYP/6-311G; reference drug protein–ligand interaction with *IT15* along with hydrophobicity and a 2D structure; reference drug protein–ligand interaction with *3EU7* along with hydrophobicity and a 2D structure; epoxybergamottin protein–ligand interaction with *IYY* along with a 2D structure; epoxybergamottin (**P28**) protein–ligand interaction with *IT29* along with hydrophobicity and a 2D structure; reference drug protein–ligand interaction with *IT29* along with hydrophobicity and a 2D structure; stigmasterol protein–ligand interaction with *3EU7* along with hydrophobicity and a 2D structure; R-stigmasterol protein–ligand interaction with *3EU7* along with hydrophobicity and a 2D structure; S-stigmasterol (S) protein–ligand interaction with *3EU7* along with hydrophobicity and a 2D structure; nobiletin (**P29**) protein–ligand interaction with *3EU7* along with hydrophobicity and a 2D structure; RMSD of complex *IT29*; radius of gyration of complex *IT29*; protein–ligand contact plot; HOMO and LUMO diagrams of (a) compound **P28** and (b) compound **P29**; optimized structure of (a) compound **P28** and (b) compound **P29**; and MEP structure and MEP scale of (a) compound **P28** and (b) compound **P29** (PDF)

■ AUTHOR INFORMATION

Corresponding Authors

Nusrat Shafiq – Synthetic and Natural Products Discovery (SNPD) Laboratory, Department of Chemistry, Government College Women University, Faisalabad 38000, Pakistan; orcid.org/0000-0002-3270-4227; Email: dr.nusratshafiq@gcwuf.edu.pk

Musaab Daelbait – Department of Scientific Translation, Faculty of Translation, University of Bahri, Khartoum 11111, Sudan; orcid.org/0009-0003-0685-8243; Email: musaabelnaim@gmail.com

Authors

Mehreen Zia – Synthetic and Natural Products Discovery (SNPD) Laboratory, Department of Chemistry, Government College Women University, Faisalabad 38000, Pakistan

Shagufta Parveen – Synthetic and Natural Products Discovery (SNPD) Laboratory, Department of Chemistry, Government College Women University, Faisalabad 38000, Pakistan

Maryam Rashid – Synthetic and Natural Products Discovery (SNPD) Laboratory, Department of Chemistry, Government College Women University, Faisalabad 38000, Pakistan

Ariba Farooq – Department of Chemistry, University of Lahore, Lahore 54000, Pakistan

Muhammad Shahab – State Key Laboratories of Chemical Resources Engineering, Beijing University of Chemical Technology, Beijing 100029, P. R. China

Ahmad Mohammad Salamatullah – Department of Food Science & Nutrition, College of Food and Agricultural Sciences, King Saud University, Riyadh 11451, Saudi Arabia

Simone Brogi – Department of Pharmacy, Pisa University, Pisa 56124, Italy; orcid.org/0000-0001-9375-6242

Mohammed Bourhia – Department of Chemistry and Biochemistry, Faculty of Medicine and Pharmacy, Ibn Zohr University, Laayoune 70000, Morocco; Laboratory of Chemistry-Biochemistry, Environment, Nutrition, and Health, Faculty of Medicine and Pharmacy, University Hassan II, Casablanca, Morocco

Complete contact information is available at: <https://pubs.acs.org/doi/10.1021/acsomega.3c05098>

Author Contributions

M.Z.: formal analysis and investigations; S.P.: writing the original draft and formal analysis; N.S. and M.S.: conceptualization, drafting, supervision, molecular docking, MD simulation study, and funding; M.R.: reviewing and editing, data validation, and supervision; A.F.: writing the original draft; M.D., A.M.S., S.B., and M.B.: reviewing and editing, data validation, and data curation.

Notes

The authors declare no competing financial interest.

■ ACKNOWLEDGMENTS

The authors are thankful to the Pakistan Science Foundation (CRP/PSF/TH-22). The authors would like to extend their sincere appreciation to the Researchers Supporting Project, King Saud University, Riyadh, Saudi Arabia, for funding this work through project number (RSP-2024R437).

■ REFERENCES

- Bhardwaj, P.; Biswas, G.; Bhunia, B. Docking-based inverse virtual screening strategy for identification of novel protein targets for triclosan. *Chemosphere* **2019**, *235*, 976–984.
- Ko, J.-H.; Arfuso, F.; Sethi, G.; et al. Pharmacological utilization of bergamottin, derived from grapefruits, in cancer prevention and therapy. *Int. J. Mol. Sci.* **2018**, *19* (12), 4048.
- Liu, J. et al. Nobiletin inhibits breast cancer via p38 mitogen-activated protein kinase, nuclear transcription factor- κ B, and nuclear factor erythroid 2-related factor 2 pathways in MCF-7 cells. *Food Nutr. Res.* **2018**; Vol. 62 DOI: 10.29219/fnr.v62.1323.
- Crowell, J. A. The chemopreventive agent development research program in the Division of Cancer Prevention of the US National Cancer Institute: an overview. *Eur. J. Cancer* **2005**, *41* (13), 1889–1910.
- Sharma, G. N.; et al. Various types and management of breast cancer: an overview. *J. Adv. Pharm. Technol. Res.* **2010**, *1* (2), 109–126.
- Foulkes, W. D.; Shuen, A. Y. In brief: BRCA1 and BRCA2. *J. Pathol.* **2013**, *230* (4), 347–349.
- Wooster, R.; Neuhausen, S. L.; Mangion, J.; et al. Localization of a breast cancer susceptibility gene, BRCA2, to chromosome 13q12–13. *Science* **1994**, *265* (5181), 2088–2090.
- Bhardwaj, P.; Iyengar, N. M.; Zahid, H.; et al. Obesity promotes breast epithelium DNA damage in women carrying a germline mutation in BRCA1 or BRCA2. *Sci. Transl. Med.* **2023**, *15* (684), No. eade1857.
- Rajan, A.; Nadhan, R.; Latha, N. R.; et al. Deregulated estrogen receptor signaling and DNA damage response in breast tumorigenesis. *Biochim. Biophys. Acta, Rev. Cancer* **2021**, *1875* (1), No. 188482.
- Metcalf, K.; Lubinski, J.; Lynch, H. T.; et al. Family history of cancer and cancer risks in women with BRCA1 or BRCA2 mutations. *J. Natl. Cancer Inst.* **2010**, *102* (24), 1874–1878.

- (11) Scully, R.; Livingston, D. M. In search of the tumour-suppressor functions of BRCA1 and BRCA2. *Nature* **2000**, *408* (6811), 429–432.
- (12) Prakash, R.; Zhang, Y.; Feng, W.; et al. Homologous recombination and human health: the roles of BRCA1, BRCA2, and associated proteins. *Cold Spring Harbor Perspect. Biol.* **2015**, *7* (4), No. a016600.
- (13) Hu, X.; Huang, W.; Fan, M. Emerging therapies for breast cancer. *J. Hematol. Oncol.* **2017**, *10* (1), No. 98.
- (14) Steduto, P. et al. *Crop Yield Response to Water*; Food and Agriculture Organization of the United Nations Rome, 2012; Vol. 1028.
- (15) Dongre, P.; Doifode, C.; Choudhary, S.; et al. Botanical Description, Chemical Composition, Traditional Uses and Pharmacology of *Citrus sinensis*: An Updated Review. *Pharm. Res.* **2023**, *8*, No. 100272.
- (16) Goudeau, D.; Uratsu, S. L.; Inoue, K.; et al. Tuning the orchestra: Selective gene regulation and orange fruit quality. *Plant Sci.* **2008**, *174* (3), 310–320.
- (17) Al Juhaimi, F.; Özcan, M. M.; Uslu, N.; et al. The effect of drying temperatures on antioxidant activity, phenolic compounds, fatty acid composition and tocopherol contents in citrus seed and oils. *Journal of food science and technology* **2018**, *55* (1), 190–197.
- (18) Adham, A. N.; Abdelfatah, S.; Naqishbandi, A.; et al. Transcriptomics, molecular docking, and cross-resistance profiling of nobiletin in cancer cells and synergistic interaction with doxorubicin upon SOX5 transfection. *Phytomedicine* **2022**, *100*, No. 154064.
- (19) Jorge, N.; da Silva, A. C.; Aranha, C. P. Antioxidant activity of oils extracted from orange (*Citrus sinensis*) seeds. *An. Acad. Bras. Ciênc.* **2016**, *88*, 951–958.
- (20) Haroen, U.; Budiansyah, A.; Nelwida, N. Phytochemical Screening and in vitro Antimicrobial Effect of Orange (*Citrus sinensis*) Ethyl Acetate Extract Silage. *Pak. J. Nutr.* **2018**, *17* (5), 214–218.
- (21) Reddy, B. A.; Priya, V. V.; Gayathri, R. Comparative phytochemical analysis and total phenolic content of citrus seed extract (*Citrus sinensis* and *Citrus limon*). *Drug Invent. Today* **2018**, *10* (10), 2038–2040.
- (22) Mary, O. B.; et al. Phytochemicals and phyto-disinfectant properties of citrus species (*Citrus limon*, *Citrus aurantifolia* and *Citrus sinensis*) for pond water purification. *GSC Biol. Pharm. Sci.* **2019**, *8* (2), 34–44, DOI: 10.30574/gscbps.2019.8.2.0139.
- (23) Gowtham, M.; et al. Toxicity of methanolic fruit peel and seed extracts from *Citrus sinensis* (L.) Osbeck against papaya mealybug, *Paracoccus marginatus* (Williams and Granara de Willink). *IJCS* **2019**, *7* (4), 804–808.
- (24) Xu, X.; Zhou, Y.; Wang, B.; et al. Genome-wide identification and characterization of laccase gene family in *Citrus sinensis*. *Gene* **2019**, *689*, 114–123.
- (25) Uzama, D.; et al. The Study of Phytochemicals, Proximate and Mineral Contents of Sweet Orange Seeds and Peels. *Nigerian J. Chem. Res.* **2021**, *26* (1), 25–32.
- (26) del Carmen Quintal Bojórquez, N.; Campos, M. R. Traditional and Novel Computer-Aided Drug Design (CADD) Approaches in the Anticancer Drug Discovery Process. *Curr. Cancer Drug Targets* **2023**, *23* (5), 333–345.
- (27) Bassani, D.; Moro, S. Past, Present, and Future Perspectives on Computer-Aided Drug Design Methodologies. *Molecules* **2023**, *28* (9), 3906.
- (28) Rajiv Gandhi, G.; Sharanya, C. S.; Jayanandan, A.; et al. Multitargeted molecular docking and dynamics simulation studies of flavonoids and volatile components from the peel of *Citrus sinensis* L. (Osbeck) against specific tumor protein markers. *J. Biomol. Struct. Dyn.* **2023**, *1* (1), 1–20.
- (29) Song, C. M.; Lim, S. J.; Tong, J. C. Recent advances in computer-aided drug design. *Briefings Bioinf.* **2009**, *10* (5), 579–591.
- (30) Macalino, S. J. Y.; Gosu, V.; Hong, S.; et al. Role of computer-aided drug design in modern drug discovery. *Arch. Pharm. Res.* **2015**, *38* (9), 1686–1701.
- (31) Maulydia, N. B.; et al. Analysis of flavonoid compounds of Orange (*Citrus* sp.) peel as anti-main protease of SARS-CoV-2: A molecular docking study. *IOP Conf. Ser.: Earth Environ. Sci.* **2021**, *951* (3), No. 012078.
- (32) Ece, A. Computer-aided drug design. *BMC Chem.* **2023**, *17* (1), No. 26.
- (33) Ayaz, M.; Sadiq, A.; Wadood, A.; et al. Cytotoxicity and molecular docking studies on phytosterols isolated from *Polygonum hydropiper* L. *Steroids* **2019**, *141* (1), 30–35.
- (34) Rajiv Gandhi, G.; Sharanya, C. S.; Jayanandan, A.; et al. Multitargeted molecular docking and dynamics simulation studies of flavonoids and volatile components from the peel of *Citrus sinensis* L. (Osbeck) against specific tumor protein markers. *J. Biomol. Struct. Dyn.* **2023**, 1–30.
- (35) Ayaz, M.; Sadiq, A.; Wadood, A.; et al. Cytotoxicity and molecular docking studies on phytosterols isolated from *Polygonum hydropiper* L. *Steroids* **2019**, *141*, 30–35.
- (36) Andole, S.; Thumma, G.; Alavala, R. R.; et al. Field-based 3D-QSAR for tyrosine protein kinase JAK-2 inhibitors. *J. Biomol. Struct. Dyn.* **2023**, 1–13.
- (37) Rashid, M.; Maqbool, A.; Shafiq, N.; et al. The combination of multi-approach studies to explore the potential therapeutic mechanisms of imidazole derivatives as an MCF-7 inhibitor in therapeutic strategies. *Front. Chem.* **2023**, *11*, No. 1197665, DOI: 10.3389/fchem.2023.1197665.
- (38) Alam, S.; Khan, F. 3D-QSAR studies on Maslinic acid analogs for Anticancer activity against Breast Cancer cell line MCF-7. *Sci. Rep.* **2017**, *7* (1), No. 6019.
- (39) Ghaleb, A.; Aouidate, A.; Ayouchia, H. B. E.; et al. In silico molecular investigations of pyridine N-Oxide compounds as potential inhibitors of SARS-CoV-2: 3D QSAR, molecular docking modeling, and ADMET screening. *J. Biomol. Struct. Dyn.* **2022**, *40* (1), 143–153.
- (40) Burley, S. K.; Bhikadiya, C.; Bi, C.; et al. RCSB Protein Data Bank (RCSB.org): delivery of experimentally-determined PDB structures alongside one million computed structure models of proteins from artificial intelligence/machine learning. *Nucleic Acids Res.* **2023**, *51* (D1), D488–D508.
- (41) Keshavarz, F.; Barbiellini, B. Application of molecular docking simulation to screening of metal–organic frameworks. *Comput. Mater. Sci.* **2023**, *226*, No. 112257.
- (42) Zarren, G.; Shafiq, N.; Arshad, U.; et al. Copper-catalyzed one-pot relay synthesis of anthraquinone based pyrimidine derivative as a probe for antioxidant and antidiabetic activity. *J. Mol. Struct.* **2021**, *1227*, No. 129668.
- (43) Dawood, S.; Zarina, S.; Bano, S. Docking studies of antidepressants against single crystal structure of tryptophan 2, 3-dioxygenase using Molegro Virtual Docker software. *Pak J. Pharm. Sci.* **2014**, *27* (5), 1529–1539.
- (44) Sarkar, A.; Santra, D.; Sundar Panja, A.; et al. Immunoinformatics and MD-simulation data suggest that Omicron spike epitopes are more interacting to IgG via better MHC recognition than Delta variant. *Int. Immunopharmacol.* **2023**, *123*, No. 110636.
- (45) Aldossari, R. M.; Ali, A.; Rehman, M. U.; et al. Computational Approaches for Identification of Potential Plant Bioactives as Novel G6PD Inhibitors Using Advanced Tools and Databases. *Molecules* **2023**, *28* (7), 3018.
- (46) Kumar, B. K.; Sekhar, K. V. G. C.; Ojha, R.; et al. Pharmacophore based virtual screening, molecular docking, molecular dynamics and MM-GBSA approach for identification of prospective SARS-CoV-2 inhibitor from natural product databases. *J. Biomol. Struct. Dyn.* **2022**, *40* (3), 1363–1386.
- (47) Pires, D. E. V.; Blundell, T. L.; Ascher, D. B. pkCSM: predicting small-molecule pharmacokinetic and toxicity properties using graph-based signatures. *J. Med. Chem.* **2015**, *58* (9), 4066–4072.
- (48) Vennila, P.; Al-Otaibi, J. S.; Venkatesh, G.; et al. Structural, spectral, molecular docking, and molecular dynamics simulations of phenylthiophene-2-carboxylate compounds as potential anticancer agents. *Polycyclic Aromat. Compd.* **2023**, 1–23.

- (49) Alam, S.; Khan, F. 3D-QSAR, Docking, ADME/Tox studies on Flavone analogs reveal anticancer activity through Tankyrase inhibition. *Sci. Rep.* **2019**, *9* (1), No. 5414.
- (50) Batalini, F.; Xiong, N.; Tayob, N.; et al. Phase 1b clinical trial with alpelisib plus olaparib for patients with advanced triple-negative breast cancer. *Clin. Cancer Res.* **2022**, *28* (8), 1493–1499.
- (51) Zayed, A.; Badawy, M. T.; Farag, M. A. Valorization and extraction optimization of Citrus seeds for food and functional food applications. *Food Chem.* **2021**, *355*, No. 129609.
- (52) Aydeniz-Guneser, B. Cold pressed orange (*Citrus sinensis*) oil. In *Cold Pressed Oils*; Elsevier, 2020; pp 129–146.
- (53) Mahato, N.; et al. Modern Extraction and Purification Techniques for Obtaining High Purity Food-Grade Bioactive Compounds and Value-Added Co-Products from Citrus Wastes. *Foods* **2019**, *8* (11), 523.
- (54) Esfahani, S. N.; et al. Synthesis of some novel coumarin isoxazol sulfonamide hybrid compounds, 3D-QSAR studies, and antibacterial evaluation. *Sci. rep.* **2021**, *11* (1), No. 20088.
- (55) Kalhotra, P.; Chittepu, V. C. S. R.; Osorio-Revilla, G.; et al. Field-template, QSAR, ensemble molecular docking, and 3D-RISM solvation studies expose potential of FDA-approved marine drugs as SARS-CoVID-2 main protease inhibitors. *Molecules* **2021**, *26* (4), 936.
- (56) Bitencourt-Ferreira, G.; de Azevedo, W. F. Molegro virtual docker for docking. In *Docking Screens for Drug Discovery*; Springer: New York, 2019; Vol. 2053, pp 149–167 DOI: 10.1007/978-1-4939-9752-7_10.
- (57) Sumera; Anwer, F.; Waseem, M.; et al. Molecular docking and molecular dynamics studies reveal secretory proteins as novel targets of Temozolomide in glioblastoma multiforme. *Molecules* **2022**, *27* (21), 7198.
- (58) Sengupta, S.; et al. In-Silico Modelling of 1- 3- [3-(Substituted Phenyl) Prop-2-Enoyl] Phenyl Thiourea Against Anti-Inflammatory Drug Targets. *Biosci. Biotechnol. Res. Asia* **2022**, *18* (2), 413–421.
- (59) Santra, D.; Maiti, S. Molecular dynamic simulation suggests stronger interaction of Omicron-spike with ACE2 than wild but weaker than Delta SARS-CoV-2 can be blocked by engineered S1-RBD fraction. *Struct Chem.* **2022**, *33* (5), 1755–1769.
- (60) Sumera; Anwer, F.; Waseem, M.; et al. Molecular Docking and Molecular Dynamics Studies Reveal Secretory Proteins as Novel Targets of Temozolomide in Glioblastoma Multiforme. *Molecules* **2022**, *27* (21), 7198.
- (61) López-Blanco, J. R.; Aliaga, J. I.; Quintana-Ortí, E. S.; et al. iMODS: internal coordinates normal mode analysis server. *Nucleic Acids Res.* **2014**, *42* (W1), W271–W276.
- (62) Attiq, N.; Arshad, U.; Brogi, S.; et al. Exploring the anti-SARS-CoV-2 main protease potential of FDA approved marine drugs using integrated machine learning templates as predictive tools. *Int. J. Biol. Macromol.* **2022**, *220*, 1415–1428.
- (63) Muddagoni, N.; et al. Homology modeling, virtual screening, prime-MMGBSA, AutoDock-identification of inhibitors of FGR protein. *Biointerface Res. Appl. Chem.* **2021**, *11* (4), 11088–11103.
- (64) Zamzami, M. A. Molecular docking, molecular dynamics simulation and MM-GBSA studies of the activity of glycyrrhizin relevant substructures on SARS-CoV-2 RNA-dependent-RNA polymerase. *J. Biomol. Struct. Dyn.* **2023**, *41* (5), 1846–1858.
- (65) Nidhi, P.; Rolta, R.; Kumar, V.; et al. Synergistic potential of Citrus aurantium L. essential oil with antibiotics against *Candida albicans*. *J. Ethnopharmacol.* **2020**, *262*, No. 113135.
- (66) Tiwari, A.; Tiwari, V.; Sharma, A.; et al. Tanshinone-I for the treatment of uterine fibroids: Molecular docking, simulation, and density functional theory investigations. *Saudi Pharm. J.* **2023**, *31* (6), 1061–1076.
- (67) Abdelrheem, D. A.; Rahman, A. A.; Elsayed, K. N.; et al. Isolation, characterization, in vitro anticancer activity, dft calculations, molecular docking, bioactivity score, drug-likeness and admet studies of eight phytoconstituents from brown alga sargassum platycarpum. *J. Mol. Struct.* **2021**, *1225*, No. 129245.
- (68) Sayin, K.; Üngördü, A. Investigation of anticancer properties of caffeinated complexes via computational chemistry methods. *Spec-trochim. Acta, Part A* **2018**, *193*, 147–155.